ACS Catalysis

pubs.acs.org/acscatalysis

Research Article

Influence of the Mn Promoter on the Composition and Activity of the Adsorbed Phase in the Carbon Paths of the CO Hydrogenation Reaction on 20 wt % Co/MnO$_x$-Al$_2$O$_3$: An Operando-SSITKA and Transient Kinetic Study

Michalis A. Vasiliades, Denzil Moodley, Renier Crous, Jana Potgieter, Thys Botha, and Angelos M. Efstathiou*

Cite This: *ACS Catal.* 2025, 15, 5318−5338

Read Online

ACCESS | Metrics & More | Article Recommendations | Supporting Information

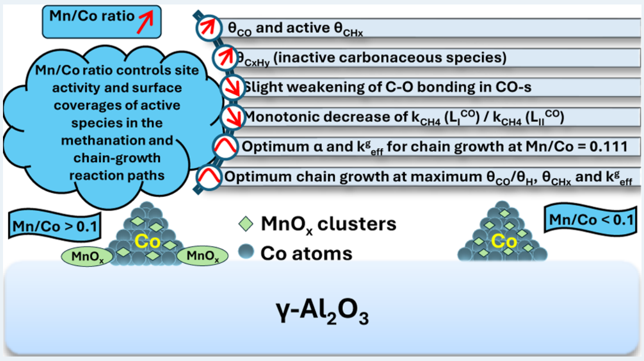

ABSTRACT: Herein, we explored the influence of the Mn/Co molar ratio (0.011−0.268) on the composition and activity of the adsorbed phase established during CO hydrogenation at 230 °C (P_T = 1.2 bar) over a 20 wt % Co/MnO$_x$-Al$_2$O$_3$ industrially relevant catalyst as a function of time-on-stream, TOS (2−50 h). Correlations between surface coverages of active and inactive carbonaceous species, site activity (k, s^{-1}) for methanation and chain growth, and the Mn/Co molar ratio for optimum performance were derived. ^{13}CO-SSITKA revealed that the Mn/Co molar ratio and TOS significantly influenced the dynamic net rate of CO chemisorption and that of −CH$_x$ formation, θ_{CO}, θ_{CHx}, TOF$_{CH4}$, and k (s^{-1}) of methanation and chain growth kinetic parameters in a diverse way. An optimum Mn/Co ratio of 0.111 was found for chain growth (C$_2$−C$_5$ hydrocarbons) and which was related to the dependence of θ_{CO} and θ_{CHx} on the Mn/Co ratio. Dynamic hydrogen chemisorption at 100 °C and H$_2$-TPD studies indicated the increase of θ_H and alteration of H-chemisorption site distribution with increasing Mn/Co ratio. *Operando* DRIFTS-mass spectrometry transient hydrogenation of two linear type adsorbed CO-s revealed the influence of Mn/Co ratio on their relative hydrogenation activity (k), highlighting the importance of the population of CO chemisorption sites of lower hydrogenation activity toward methane. Structural and topological information for the presence of the MnO$_x$ promoter in Co/γ-Al$_2$O$_3$ was obtained via HRTEM/EDX (RGB mapping). Highly dispersed MnO$_x$ clusters were formed on the cobalt surface for low Mn/Co ratios (ca. 0.011), while for higher Mn/Co ratios both MnO$_x$ particles surrounded the Co particles (10−12 nm) and Mn chemically interacted with the Co surface (e.g., Co-MnO clusters and agglomerates). It is proposed that optimum chain growth is the result of a balance between unpromoted and Mn-promoted cobalt surface regions for the present 20 wt % Co/MnO$_x$-Al$_2$O$_3$ catalytic system. This work paved the way for deriving reliable correlations between important kinetic parameters of CO hydrogenation that control the chain growth in FTS for Mn-based and other promoted Co-based FTS catalysts.

KEYWORDS: *CO hydrogenation, Mn-promoted Co/Al$_2$O$_3$, ^{13}CO-SSITKA, operando DRIFTS-MS methodology, DRIFTS transient CO hydrogenation, Mn/Co surface coverage relationships*

1. INTRODUCTION

Fischer−Tropsch synthesis (FTS) involves the catalytic conversion of syngas (CO/H$_2$ or CO/CO$_2$/H$_2$), primarily derived from natural gas, coal, biomass or renewable sources via the steam reforming and water−gas shift reactions, into high value-added products, namely: olefins, higher alcohols, and long-chain hydrocarbons (n (CO + 2H$_2$) → (−CH$_2$)n + nH$_2$O; ΔH° = −167 kJ mol^{-1}).[1−6] The Fischer−Tropsch synthesis is industrially operated using promoted supported cobalt catalysts on basic metal oxide(s) carriers, predominantly toward C$_{4+}$-hydrocarbons. To advance the design of such FTS industrial catalysts, the finding of relationships between catalyst structural properties and intrinsic kinetic parameters related to site activity (k, s^{-1}) and surface composition of the active phase under operating reaction conditions becomes very important.[7,8] Substantial attention has already been given to

Received: December 23, 2024
Revised: February 20, 2025
Accepted: March 10, 2025

ACS Publications

https://doi.org/10.1021/acscatal.4c07921

comprehending the FTS mechanism, encompassing microkinetic analysis.[6,9−12]

Cobalt-based catalysts supported on metal oxides (e.g., Al_2O_3, SiO_2, TiO_2) and promoted with small amounts of noble (e.g., Pt, Re, Ru) and other metals (e.g., Mn, La, K) have been explored.[13−20] In general, promoters are commonly categorized into three distinct groups, namely: (i) structural, (ii) electronic, and (iii) dual structural-electronic promoters.[21−23] Structural promoters primarily influence the formation and stability of the active phase, whereas electronic promoters influence the kinetics of elementary reaction steps by altering the local electronic structure of active sites, either by introducing or withdrawing electron density near the Fermi level in the valence band of the active metal (e.g., cobalt), thus impacting the energetics of chemisorption and surface reaction processes, and thus surface coverages.[7,22,23] Dual structural-electronic promoters combine aspects of both structural and electronic promotion. They integrate with the active metal phase and can induce structural changes which cause alterations in the electronic structure of the active sites.[22,24−27]

The dual electronic and structural promotional role of Mn introduced into supported Co catalysts was highlighted.[28−34] Ma and his group[32] have recently proposed a carbon-mediated strategy to construct a robust nanointerfacial Co-MnO_x-(C)/SiO_2 catalyst. The resulting small Co_3O_4 particles (∼ 6 nm) endowed with abundant surface oxygen vacancies facilitated the dispersion and anchoring of MnO_x species, where stable and rich Co-MnO_x nanointerfaces were obtained after H_2 reduction and CO/H_2 reaction conditions, leading to high STY of C_{2+}-olefins and olefin/paraffin ratios. It was shown that these nanointerfaces provided high surface coverage ratio of CO-s/H-s under FTS conditions, which enhanced the rate of carbon-chain growth and β-H elimination while suppressing olefin hydrogenation. The same research group reported earlier[35] the tuning of geometric and electronic structure of interfacial Ni-based FTS catalyst by the immobilization of disordered $TiO_{2\text{-x}}$ overlayers onto the surface of Ni nanoparticles. As a result of this, $Ni^{\delta\text{-}}$/$TiO_{2\text{-x}}$ site was very efficient for CO activation and CH−CH coupling toward C_2H_4 formation at 1 atm pressure, whereas Ni metal sites promote hydrogenation of C_2H_4 toward C_2H_6.

Mn as a structural promoter was found to enhance Co dispersion by impeding Co particle agglomeration and facilitating cobalt oxide reduction. On the other hand, excessive Mn loading decreases Co dispersion (increase of Co particle size) due to pore blocking effects.[7,36,37] Recently, Koshy et al.[8] using scanning nanobeam diffraction (nm-resolved structure and crystal phase information), illustrated the evolution of Co nanoparticles structure from the tetragonal $Co_{3\text{-x}}Mn_xO_4$ spinel in the as prepared and calcined nonporous alumina-supported and Mn-promoted Co to adjacent Co_3O_4 and MnO_2 regions in the postreaction. Also, STEM/EDS mapping revealed highly dispersed Co and Mn oxide nanoparticles in the calcined catalyst but Co-rich and Mn-rich regions adjacent to each other after reaction. de Jong's group[38] prepared a Co−Pt/MnO-SiO_2 catalyst with 0.08 Mn/Co molar ratio which showed an increased C_{5+}-selectivity, in agreement to a later work reported by Johnson and Bell,[39] due to an enhanced surface coverage of active $-CH_x$ intermediates responsible for a higher chain-growth probability (α) with minimal activity loss. Infrared spectroscopic CO adsorption studies revealed that MnO induced the formation of cobalt surfaces with low-index crystallographic planes or steps and corners with relatively low coordination number as compared to the unpromoted Co−Pt/SiO_2 catalyst.[38] SSITKA studies revealed that the surface concentration of reversibly chemisorbed CO and its mean residence time decreased, while the same kinetic parameters for the $-CH_x$ *active* intermediate were increased with increasing MnO loading.[39] On the other hand, the impact of Mn promotion on essential intrinsic kinetic parameters (i.e., θ and k) related to (i) the H_2 chemisorption and CO dissociation steps, (ii) the -C_xH_y formation steps (chain growth reaction path), and (iii) the formation of inactive carbonaceous species contributing to catalyst deactivation remains largely unexplored.

Recently, Potgieter et al.[40] pointed out that FTS presents an attractive avenue to produce sustainable aviation fuels (SAF) from various renewable feedstocks.[41] Mn- and Ti-promoted Co on alumina was successfully developed and optimized (Mn/Co and Ti/Co) for FTS at 20 bar in lab-scale and pilot plant operating conditions.[40] A Mn/Co molar ratio of 0.11 was found to be optimum, a result that is remarkably similar to that of the present transient isotopic kinetic study of CO hydrogenation at 1.2 bar.

Few studies investigated the chemical nature and surface coverage of active and inactive carbonaceous species (related to catalyst deactivation) on supported and promoted Co-based catalysts using *operando* transient kinetic and isotopic techniques.[28,42−55] Steady-State Isotopic Transient Kinetic Analysis (SSITKA) is recognized as a powerful technique for estimating important kinetic parameters, e.g., the concentration (μmol g^{-1} or θ) and mean residence time (τ, s) of *active* intermediates, and the intrinsic site activity (k, s^{-1}) of the rate-determining step (RDS) of industrially relevant catalysts without the need to apply a microkinetic modeling or to assume a given surface structure for the active catalytic phase (e.g., DFT computations).[49,54−57] When SSITKA is used in an *operando* methodology (e.g., SSITKA-DRIFTS-Mass spectrometry), the chemical structure of active and inactive species can also be identified.[58−62]

We report here the influence of the Mn/Co molar ratio on the composition of the adsorbed phase established during CO hydrogenation at 230 °C (2−50 h time-on-stream) over an industrially relevant 20 wt % Co/γ-Al_2O_3 (Sasol) FTS catalyst using SSITKA and other transient kinetic experiments. In particular, the influence of Mn/Co ratio on: (i) the dynamic rates of CO-s chemisorption, formation and reaction of *active* CH_xO-s (C_α), (ii) the concentration (μmol g^{-1} and θ) and mean residence time (τ, s) of CO-s and active CH_xO-s intermediates formed during CO hydrogenation (low CO-conversion), (iii) the turnover frequency (s^{-1}) of CH_4 formation based on the total Co surface metal atoms (TOF_{CH4}, s^{-1}), and (iv) the relative activity (k, s^{-1}) toward CH_4 formation of two linear-type adsorbed CO-s formed during CO hydrogenation at 230 °C (*operando* DRIFTS-MS transient isothermal hydrogenation combined with kinetic modeling) was investigated. The concentration of *inactive* adsorbed $-C_xH_y$ species (C_β) formed during the CO/H_2 reaction, and which are hydrogenated (50% H_2/He) at 230 °C, ″soft″ carbon, and that of *inactive* refractory carbonaceous species (C_γ) hydrogenated at $T > 230$ °C, ″hard″ carbon, were also determined. This work is relevant to FTS process at higher than 1 bar pressure since the RDS of the latter process is largely controlled by the formation of CH_x-s intermediates than by chain growth reaction steps.[28,63−65]

2. MATERIALS AND METHODS

2.1. Synthesis and Activation of Co/MnO_x-Al_2O_3 Catalysts. Puralox 2/150 alumina (Sasol) was impregnated with a solution of manganese acetate in water of appropriate concentration to give Mn loadings in the 0.3−7.5 wt % range or Mn/Co molar ratio in the 0.011−0.268 range. The dried material was then calcined in static air for 5 h in a furnace at 550 °C. For the conventional preparation of 20 wt % Co-0.05 wt % Pt/x wt % Mn - Al_2O_3, a slurry impregnation of the Mn-modified γ-Al_2O_3 support with an aqueous cobalt nitrate solution containing also the platinum precursor (ammonium platinum nitrate) was applied in a rotary evaporator under reduced pressure. After impregnation and drying, the catalyst sample was calcined at 250 °C in static air for 5 h. To achieve the required cobalt loading of 20 wt %, two impregnation and calcination steps were performed.

Co-impregnation was not considered, aiming to focus specifically on the interactions between Co and Mn for a series of MnO_x-alumina as the Mn/Co ratio increased. This approach aimed to eliminate any additional interactions that might have been introduced by coimpregnation of Mn with Co. The latter preparation method has been observed to lead to dealloying during reduction as well as changes in Co crystallite size compared to the methodology employed in the present work.[66]

Before any catalytic and transient kinetic experiments were conducted, the solid material in powdered form was sieved to a particle size of less than 106 μm. This step was taken to minimize internal mass transport resistances (see Section 2.5). A CSTR microreactor made of quartz was used in all experiments.[67] After the catalyst sample was loaded in the microreactor, the temperature of the catalyst was increased at the rate of $\beta = 1$ °C min^{-1} in H_2 gas-flow (50 N mL min^{-1}) to 425 °C and kept at this temperature for 16 h (activation step). It is noteworthy that the degree of reduction (DOR, %) of Co_3O_4 to metallic Co for the unpromoted and Mn-promoted 20 wt % Co-0.05 wt % Pt/γ-Al_2O_3 catalyst was estimated via transient isothermal oxidation,[49] and this was found to be in the range between 94 and 98%. The DOR (%) of cobalt oxide in each catalyst composition was considered for the estimation of the mean Co particle size and dispersion.

2.2. Characterization of Structural Properties of Co/MnO_x-Al_2O_3. Several structural characteristics of the calcined Co/x wt % Mn−Al_2O_3 solid materials were examined using High-Resolution Transmission Electron Microscopy (HR-TEM). The TEM analysis was conducted by using a Titan 80-300 ST electron microscope operating at 300 kV and equipped with a spherical aberration corrector (Cs corrector) for improved image quality (CEOS CETCOR) and an energy filter (GIF Quantum 963, Gatan, Inc.). To prepare samples for TEM analysis, selected powdered specimens were dispersed in ethanol and then drop-cast onto carbon-coated copper grids (200 mesh). This preparation procedure allowed for high-resolution imaging in TEM mode, structural analysis using Selected Area Electron Diffraction (SAED), and elemental mapping using energy-dispersive X-ray (EDX) spectroscopy. To achieve nanoscale elemental mapping, Electron Energy Loss Spectroscopy (EELS) was employed in conjunction with Scanning Transmission Electron Microscopy (STEM). The entire process of acquiring TEM data and subsequent postprocessing was conducted using Gatan Microscopy Suite (GMS) software (v. 3.2).

2.3. Hydrogen Transient Isothermal Chemisorption (H_2-TIC) and Temperature-Programmed Desorption (H_2-TPD). Transient isothermal chemisorption of hydrogen (H_2-TIC) at 100 °C followed by temperature-programmed desorption (H_2-TPD) were conducted to investigate the influence of Mn/Co ratio on the heterogeneity of cobalt surface in H_2 chemisorption sites, namely, the surface concentration and quality of sites (binding strength between Co_s and H, E_{Co-H}), and the dynamics of hydrogen chemisorption. A hydrogen partial pressure of 4.5 Torr (0.5 vol % H_2/He) and an adsorption temperature of 100 °C were used to account for likely activated hydrogen chemisorption on the cobalt surface of Co/MnO_x-Al_2O_3 and to minimize hydrogen spillover.[68]

An amount of 0.1 g of catalyst was mixed with SiC (1:1 w/w) and introduced into the CSTR microreactor, followed by the activation procedure outlined in the previous section. H_2 reduction ($P_{H2} = 1$ bar) was then carried out at 425 °C for 2 h. The temperature of the catalyst was then increased to 600 °C in He-gas flow to desorb any hydrogen that might have spilled over onto the support. The temperature was subsequently lowered to 100 °C, and a step-gas switch from He to 0.5 vol % H_2/1 vol % Kr/Ar/He ($F_T = 50$ N mL min^{-1}) was made (H_2-TIC) until no H_2 consumption was observed. The temperature of the catalyst was subsequently decreased to 30 °C in the 0.5% H_2/He gas mixture and kept at 30 °C for 5 min, followed by a He purge (5 min) and a TPD run to 600 °C (50 N mL min^{-1}, $\beta = 30$ °C min^{-1}). During H_2-TIC, online quadrupole mass spectrometer (QMS, Balzers, Omnistar 1−200 amu) was monitoring the H_2 and Kr signals (m/z = 2 and 84, respectively). The H_2 signal was monitored and converted into mol % or ppm using a certified 0.95 vol % H_2/He gas mixture. Estimation of the dynamic rates and the respective chemisorption amounts in H_2-TIC and H_2-TPD runs are described in Supporting Information, SI (Section S1).

2.4. $^{12}CO/^{13}CO$ Isotopic Exchange at 155 °C. The surface coverage of reversibly adsorbed CO-s (θ_{CO}) in the absence of any hydrogenation activity ($X_{CO} \sim 0$) using the feed gas composition of 5 vol % CO/x vol % H_2/He (x = 0, 5, 10) at 155 °C was estimated. The purpose was to compare this θ_{CO} with that obtained under the influence of other adsorbed species formed in the CO hydrogenation at 230 °C and at X_{CO} conversion in the 20−25% range, as a function of the Mn/Co ratio (see Section 2.6). The amount (μmol of CO g^{-1}) of reversibly chemisorbed CO-s under the above-mentioned adsorption gas composition was estimated based on the amount of ^{12}CO-s exchanged for ^{13}CO(g) following the sequence of step-gas switches at 155 °C: He → 5 vol % ^{12}CO/x vol % H_2/1 vol % Kr/Ar/He (15 min) → 5 vol % ^{13}CO/x vol % H_2/He (t). During the first switch, the evolution of ^{12}CO, $^{12}CO_2$ and Kr gas response curves was monitored by MS (m/z = 28, 44 and 84, respectively). This allowed us to estimate the equivalent surface coverage of both the adsorbed CO-s and that of other derived adsorbed species at 155 °C, after considering the possible interaction of CO(g) with the catalyst surface other than its chemisorption (e.g., interaction with the OH groups of alumina support, Boudouard reaction on the cobalt surface).

In the subsequent isotopic switch to 5% ^{13}CO/x vol % H_2/He (t), the transient response curves of ^{13}CO, $^{13}CO_2$ and Kr were monitored (m/z = 29, 45 and 84, respectively), and the dynamic rate of ^{13}CO(g) consumption was estimated via a material balance. The latter can be justified based on the following three reaction steps: (i) exchange of ^{12}CO-s for ^{13}CO-s (reversible CO adsorption on the Mn-promoted cobalt surface), (ii) formation of $^{13}CO_2$ via the Boudouard reaction, and (iii) reversible reaction of ^{13}CO(g) with the −OH of alumina support toward the formation of H^{13}COO-s (formate species); CO-s + s−OH ↔ HCOO-s. After the 15 min treatment of the catalyst with ^{12}CO/x vol % H_2/He, the CO consumption was found to be small, and this was accounted for by the production of CO_2 measured. This means that practically a constant amount of HCOO was formed. The possibility of HCOO formation (reversible and/or irreversible path) discussed above was checked by in situ DRIFTS after performing the above-mentioned ^{12}CO (or ^{13}CO)/x vol % H_2/He gas treatments detailed in SI (Section S2). Also, details of the quantitative analysis performed for the ^{12}CO/^{13}CO isotopic exchange using mass spectrometry are provided in SI (Section S2).

2.5. Kinetic Analysis of ^{12}CO-s/^{13}CO-s Isotopic Exchange. The dynamic kinetic rate of exchange of preadsorbed ^{12}CO-s for ^{13}CO-s under the ^{13}CO/x vol % H_2/He isotopic switch (eq 1) can be used to illustrate the influence of Mn/Co ratio and H_2 partial pressure on the binding strength of adsorbed CO-s on the cobalt surface via the specific rate constant of desorption, k_d (s^{-1}).

$$^{12}\text{CO-s} + {}^{13}\text{CO(g)} \rightarrow {}^{12}\text{CO(g)} + {}^{13}\text{CO-s} \tag{1}$$

The dynamic rate of ^{12}CO/^{13}CO exchange (eq 1) is described by the following eq 2:

$$d\left(\frac{\theta_{12_{CO}}}{dt}\right) = -k_d y_{13_{CO}} \theta_{12_{CO}} \tag{2}$$

where the desorption rate constant, k_d (s^{-1}) for ^{12}CO-s is considered independent of θ_{CO}. In eq 2, $y_{13_{CO}}$ is the mole fraction of ^{13}CO(g) measured in the gas phase during the transient isotopic exchange experiment. In eq 2, the change in $\theta_{12_{CO}}$ with time was considered not to be largely influenced by the readsorption of ^{12}CO(g) for the following reasons. According to the experimental results to be described later, during most of the time after the switch ^{12}CO(g)/^{13}CO(g), between t_1 = 20 s and t_2 = 100 s, $y_{13_{CO}}$ varied between 0.035 and 0.05 ($y^f_{13_{CO}} = 0.05$), while $y_{12_{CO}}$ values were between 0.0125 and 0.0. Considering also that the desorption of ^{13}CO-s leaving an empty site is a more energetic process than the readsorption of ^{12}CO(g) onto that empty site, the backward reaction in eq 1 was neglected. This allowed an analytical solution for eq 2 to be obtained with an approximate solution for $\theta_{12_{CO}}(t)$ (eq 3) after considering an arithmetic average value ($y^{avg}_{13_{CO}}$) for $y_{13_{CO}}$ between t_1 and t_2.

$$\theta_{12_{CO}}(t) \cong \theta_o \exp(-k_d y^{avg}_{13_{CO}} t) \tag{3}$$

In eq 3, θ_o is the initial surface coverage of ^{12}CO-s which is estimated via eqs S3−S5. After linearization of eq 3, and using only experimental data of $\theta_{12_{CO}}$ (t) between t_1 and t_2, the specific desorption rate constant, k_d of adsorbed CO-s can be estimated:

$$\ln(\theta_{12_{CO}}) = -(k_d y^{avg}_{13_{CO}})t + \ln(\theta_o) \tag{4}$$

The $\theta_{CO}(t)$ for ^{12}CO-s was estimated via the following eq 5:

$$\theta_{CO} = \frac{N_{CO\text{-}s}}{N_{Co,surf}} \tag{5}$$

where, $N_{Co,surf}$ is the total amount of surface Co per gram of catalyst (μmol Co_s g^{-1}), and which was estimated based on the dispersion value of Co metal (HAADF-STEM measurements, see Section 3.1).

2.6. SSITKA-Mass Spectrometry (CO Hydrogenation at 230 °C). The Steady-State Isotopic Transient Kinetic Analysis (SSITKA) technique was employed to investigate the influence of the Mn/Co ratio on the carbon pathway(s) of the CO methanation reaction at 230 °C, and as a function of time-on-stream (TOS). The following step-gas isotopic switch 5 vol % ^{12}CO/10 vol % H_2/He (Δt, 230 °C) → 5 vol % ^{13}CO/10 vol % H_2/1 vol % Kr/Ar/He (t), Δt = 0.5, 2, 5, 10, 20, 30, and 50 h, was employed.[53] Notably, the chosen CO conversions were kept below 20%. The absence of both external and internal mass transport resistances within the catalyst bed and individual catalyst particles was also confirmed using established experimental methodologies.[69] It is important to note that Dinse et al.[36] reported that in the FTS at 1 bar on Co/Mn-SiO_2, the selectivity of C_2−C_4 products remained unaffected with decreasing CO conversion and varying Co/Mn molar ratio.

The SSITKA switch was initiated after pseudosteady state reaction conditions (^{12}CO/H_2/He, 230 °C) with TOS were established. During the SSITKA switch, rates of CO conversion and products formation were kept the same within better than 2%. The mass numbers (*m*/*z*) of $^{12}CH_4$ (15), $^{13}CH_4$ (17), H_2O (18), ^{12}CO (28), ^{13}CO (29) and Kr (84) were continuously monitored by MS. The analysis of the $^{13}CH_4$-MS signal carefully considered the relative contribution of *m*/*z* = 18 (H_2O) signal to that of 17 ($^{13}CH_4$), despite the fact that small amounts of water were present in both ^{12}CO/H_2 and ^{13}CO/H_2 effluent gas streams. To verify the reproducibility of experiments, the up- and down-step SSITKA switches were performed twice.

The dynamic rate of ^{13}CO exchange during the SSITKA switch depends on (i) the individual rates of ^{12}CO-s desorption and ^{13}CO(g) adsorption, and (ii) the consumption rate of ^{13}CO-s toward the formation of ^{13}C-containing gas products. These dynamic rates (μmol g^{-1} s^{-1}) of CO-s exchange (eq 6) and that of active CH_x-s intermediates leading to CH_4 (eq 7), were previously reported by us.[49] It is noted that the rate of exchange of ^{12}CO-s for ^{13}CO-s was significantly faster than the rate of exchange of $^{12}CH_x$-s for $^{13}CH_x$-s, and this reflects the fact that $Z_{13_{CO\text{-}s}} \sim Z_{13_{CO}}$.[44,49]

$$R^{ex}_{CO\text{-}s}(t) = \frac{F_T}{W} y^f_{CO}[Z_{Kr}(t) - (1 - X_{CO})Z_{CO}(t) - 2X_{CO}S_{CH_4}Z_{CH_4}(t)] \tag{6}$$

$$R^{ex}_{CHx\text{-}s}(t) = \frac{F_T}{W} y^f_{CO} X_{CO}[Z_{CO}(t) - S_{CH_4}Z_{CH_4}(t)] \tag{7}$$

In eqs 6 and 7, X_{CO} and S_{CH_4}(%) are the CO conversion and CH_4 selectivity, respectively, before the SSITKA switch, y^f_{CO} is the mole fraction of CO in the feed (0.05; 5 vol %), and Z_i refers to the dimensionless concentration of gas-phase species i (e.g., Kr, CO and CH_4). The concentration (μmol g^{-1}) of the reversibly chemisorbed CO-s and that of total *active* CH_x-s and CH_xO-s, named for simplicity CH_x-s, and which are formed in the carbon-path of methane formation, along with their corresponding surface coverages, were determined as described in SI (Section S3, eqs S10−S12).

The turnover frequency, TOF (s^{-1}) of CH_4 formation prior to the SSITKA switch was estimated based on the dispersion of Co metal (TOF_{CH4}, s^{-1}) given by eq 8, and the mean surface residence time of CH_x-s (τ_{CHx}, s) was determined using eq 9. Additionally, the effective rate constant (k_{eff}, s^{-1}) associated with the RDS of the methanation reaction was estimated using eq 10. It is considered that the RDS is one of the hydrogenation of $-CH_xO$ and $-CH_x$ intermediates.[49,70]

$$TOF_{CH_4}(s^{-1}) = \frac{F_T y_{CH4}}{W_{cat} N_{Co,surf}} = \frac{\theta_{CHx}}{\tau_{CHx}} \tag{8}$$

$$\tau_{CHx}(s) = \int_0^{t_{s.s}} [Z_{^{13}CO}(t) - Z_{^{13}CH_4}(t)]dt \tag{9}$$

$$k_{eff}(s^{-1}) = \frac{TOF_{CH_4}}{\theta_{CHx}} = \frac{1}{\tau_{CHx}} = k\theta_H \tag{10}$$

2.7. Transient Isothermal (TIH) and Temperature-Programmed Hydrogenation (TPH). Following the SSITKA switch, transient isothermal hydrogenation (TIH) and temperature-programmed hydrogenation (TPH) experiments were conducted according to the following sequence of step-gas switches: $^{13}CO/H_2/Kr/He$ (230 °C, 7 min) → He (3 min, 230 °C) → 50 vol % H_2/He (TIH, 7 min, 230 °C) → TPH to 600 °C (β = 10 °C min^{-1}). It should be noted that during the 3 min He purge, only a small amount of ^{13}CO-s was desorbed from the catalyst surface.

During TIH and TPH, the $^{12}CH_4$, $^{13}CH_4$, H_2O and Kr gases were monitored by mass spectrometry (m/z = 15, 17, 18 and 84, respectively). The $^{12}CH_4$ response recorded during TIH highlights the presence of *inactive* or *spectator* C-containing species, named C_β, which were formed during CO hydrogenation under $^{12}CO/H_2$ gas treatment. The C_β species were not able to exchange with $^{13}CO(g)$ during the subsequent $^{13}CO/H_2$ isotopic gas treatment. The response of $^{13}CH_4$ is the result of hydrogenation of both the adsorbed ^{13}CO-s and *active* $^{13}CH_x$-s (named C_α), which were exchanged during the $^{13}CO/H_2$ gas treatment. During the TPH step (>230 °C), the refractory carbonaceous *inactive* species, named C_γ (C_xH_y-s) can also be hydrogenated to CH_4. Further details of the analyses performed on TIH and TPH experiments are reported in SI (Section S4).

2.8. ^{13}CO SSITKA-DRIFTS and Transient Hydrogenation of CO-s. *In situ* DRIFTS spectra were collected by using a PerkinElmer Frontier FTIR spectrometer coupled with a high-temperature/high-pressure temperature-controllable DRIFTS reactor cell (Harrick Scientific, Praying Mantis) equipped with CaF_2 windows. About 90 mg of the passivated Co/MnO_x-Al_2O_3 catalyst (activated at 425 °C in H_2 and treated in $2\%O_2/He$ at 50 °C) was sieved to less than 106 μm, introduced into the DRIFTS cell, and then reduced in a 50% H_2/Ar gas atmosphere at 425 °C for 2 h. The DRIFTS reactor cell was subsequently cooled to 230 °C, where background spectra were recorded after a 20 min Ar gas purge.

The influence of the Mn/Co ratio on the evolution of different types of adsorbed CO-s was investigated. Changes in the relative abundance of these CO-s species as a function of Mn/Co ratio were monitored during the first 2 h of CO hydrogenation at 230 °C. DRIFTS spectra were recorded before and after the SSITKA switch: 5% $^{12}CO/10\%\ H_2/Ar$ (230 °C, 2 h) → 5% $^{13}CO/10\%\ H_2/Ar$ (230 °C, 10 min) aiming to identify adsorbed CO-s that may not actively participate in the CO hydrogenation reaction, but it could simply adsorb irreversibly on the Co surface.

The transient kinetics of hydrogenation and the reactivity of individual adsorbed CO-s (linear and bridged type) formed at 230 °C were explored using the *operando* DRIFTS-Mass Spectrometry methodology. This involved transient isothermal hydrogenation (TIH) in a 50 vol % H_2/Ar gas atmosphere, following CO hydrogenation reaction and 3 min Ar purge at 230 °C. The primary goal was to study the dynamics of hydrogenation of *individual types of CO-s* and how this is influenced by the Mn/Co molar ratio. Details of the analysis were previously reported.[49,53,71]

2.9. Steady-State Kinetic Rates of CO Hydrogenation at 230 °C. To elucidate the influence of Mn/Co molar ratio on the kinetic selectivities of the C_1−C_5 hydrocarbon products for the CO hydrogenation (5 vol % CO/10 vol % H_2/He) conducted at 1.2 bar total pressure and 230 °C, the individual carbon selectivities and chain-growth probability (α) were estimated.[49] An amount of 0.2 g of fresh catalyst was well-mixed with 0.2 g of SiC and introduced into the microreactor. After following the catalyst activation procedure previously described, the catalyst was exposed to the CO/H_2 feed gas stream for 5 h with the CO conversion (X_{CO}) remaining below 10% in all the subsequent kinetic rate measurements conducted. The effluent stream was analyzed using online Gas Chromatography (Agilent GC-7890A, equipped with two parallel columns (Agilent J&W HP Plot-Q column (19095-Q04, 30 m length, 0.530 mm inner diameter) and Agilent J&W HP-Molesieve column (19095P-MSO, 30 m length, 0.530 mm inner diameter). Both TCD and FID detectors were used for analysis.

3. RESULTS AND DISCUSSION

3.1. Characterization of Co/MnO_x-Al_2O_3 Catalysts. The Red-Blue-Green (RBG) mapping of calcined unpromoted and Mn-promoted Co/γ-Al_2O_3 catalysts depicted in Figure 1 shows the distribution of Co_3O_4 particles (Blue) deposited on the surface of x wt % Mn−Al_2O_3 supports. The RGB colors represent Al (Red), Mn (Green), and Co (Blue), respectively. The average Co_3O_4 size (d_{Co3O4}, nanometers) was determined by measuring more than 100 particles from several imaged areas. After using the relationship: d_{Co} (nm) = 0.75 d_{Co3O4}, the

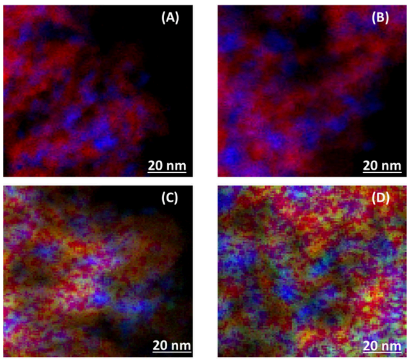

Figure 1. Red-Green-Blue (RGB) mapping analysis of the catalysts (Red: Al, Green: Mn, Blue: Co). (A) Unpromoted, (B) 0.3 wt % Mn (Mn/Co = 0.011), (C) 3.1 wt % Mn (Mn/Co = 0.111), and (D) 7.5 wt % Mn (Mn/Co = 0.268) promoted Co/γ-Al_2O_3 catalysts.

average size (nm) of cobalt particles was estimated and results are reported in Table 1. The Co dispersion was estimated using the relationship: D_{Co} (%) = ($0.96/d_{Co}$) x 100, after assuming a spherical geometry for the cobalt particles with a uniform site density of 14.6 atoms per nm^2.[72,73] The unpromoted 20 wt % Co/γ-Al_2O_3 catalyst showed lattice fringes with a *d*-spacing of 0.5741 nm (Figure S1), which corresponds to the Moire fringes of (111) and (222) planes of Al and γ-Al_2O_3, respectively.[74]

Table 1. Estimated Co Dispersion (D_{Co}, %), Average Crystallite Size (d_{Co}, nm), $N_{Co, surf}$ (μmol g^{-1}) Based on HAADF-STEM Measurements

20 wt % Co/x wt % Mn−Al_2O_3	D_{Co} (%)	d_{Co} (nm)	$N_{Co,surf}$ (μmol g^{-1})
0	9.1	10.5	324.3
0.3 (0.011)[a]	9.2	10.4	327.8
3.1 (0.111)	8.9	10.7	317.2
7.5 (0.268)	7.5	12.8	267.3

[a] Mn/Co molar ratio.

Figure 2 shows a lattice fringe of 0.4868 nm for the 0.3 wt % Mn (Mn/Co = 0.011) promoted Co/γ-Al_2O_3 catalyst, and which is correlated with the (111) plane of Co_3O_4.[75] An average size of d_{Co} = 10.4 nm was estimated using the RGB mapping (Figure 1B), which is very similar to the unpromoted 20 wt % Co/γ-Al_2O_3 catalyst. The absence of green color in Figure 1B is due to the low Mn content (0.3 wt %) in the sample. The EDX spectra presented in Figure S2 clearly confirm the presence of Mn for the higher loadings (3.1 and 7.5 wt %). According to Figure 1 and Table 1, the presence of Mn in the 0.3−7.5 wt % loading range (Mn/Co = 0.011−0.268) only slightly influenced the Co particle size (10.5−12.8 nm). The observed differences in the catalytic performance (kinetic regime) and various transient kinetic experiments on the 20 wt % Co/MnO_x-Al_2O_3 catalysts of varying Mn/Co ratio, to be reported in the following sections, are therefore unlikely to be due to particle size effects.[76]

There are two arrangements of Mn with respect to Co on the promoted catalysts. The first one refers to Mn surrounding the Co particles for the higher Mn/Co molar ratios, as revealed by the RGB mapping (Figure 1C, D), and the second arrangement refers to Mn chemically blended with Co, as shown by the cyan areas in the RGB mapping. For higher Mn/Co molar ratios, Mn species seem to diffuse on the surface, homogeneously agglomerating with Co and forming Co-MnO_x agglomerates.[8]

Tucker et al.[13] reported EDS elemental mapping for Mn-promoted Co/Al_2O_3 catalysts, indicating that Co and Mn were in proximity, in line with the present findings. Additionally, Bell and co-workers[77] reported (XRD, STEM-EDX and EELS studies) that in the case of Co/MnO-SiO_2 catalyst, most of the Mn species were found to be associated with the Co particles for Mn/Co lower than 0.1 (critical loading point) due to the inhibition of spinel phase formation.[78] Zhu et al.[32] have illustrated that the plentiful Co-MnO_x nanointerfaces formed over the Co-MnO_x/SiO_2 (HAADF-STEM, XPS, XANES studies) manipulated the surface electronic property of Co, and as a result of this, high surface coverage ratio of CO-s/H-s was established under FTS conditions, which favored olefin and olefin/paraffin yields.

Potgieter et al.[40] reported that for Co/Al_2O_3 promoted with Mn and Ti and prepared at a pilot-scale (slurry-phase impregnation), Mn formed clusters in close association with the cobalt nanocrystallites. In most cases, Mn appeared to be situated at the edges of the cobalt crystallites, partially covering them or forming enriched regions of Mn near the Co crystallites. On the other hand, Johnson et al.[39] reported the coexistence of two distinct sites on the catalytic surface, namely, the promoted sites across the interface between Co and MnO promoter, which favor C_{5+}-hydrocarbon formation, and the unpromoted sites situated on the surface of Co nanoparticles, and which accommodate H-s adsorbed species, mainly responsible for the high-pressure hydrogenation of CO-s toward lower than C_{5+}-hydrocarbons.

In the case of 3.1 wt % Mn (Mn/Co = 0.111) promoted catalyst (Figure S3), the lattice fringes with *d*-spacings of 0.2042 and 0.2366 nm correspond to the (004) and (222) planes of Co_3O_4, respectively,[75] while in the case of 7.5 wt % Mn (Mn/Co = 0.268) promoted catalyst, the *d*-spacing of 0.4052 nm corresponds to the (111) plane of Co_3O_4 (Figure S4).[75] The collected EDX spectra (Figure S2) confirmed the presence of Mn but at lower amounts than the nominal loading, ca. 1.6 and 3.2 wt % in the case of 3.1 and 7.5 wt % Mn, respectively. The latter effect is attributed to the Mn affinity for the metal oxide support (migration of Mn to the support). In the case of γ-Al_2O_3, it has been reported[79−81] that Mn was predominantly located at the interface (enhancing its

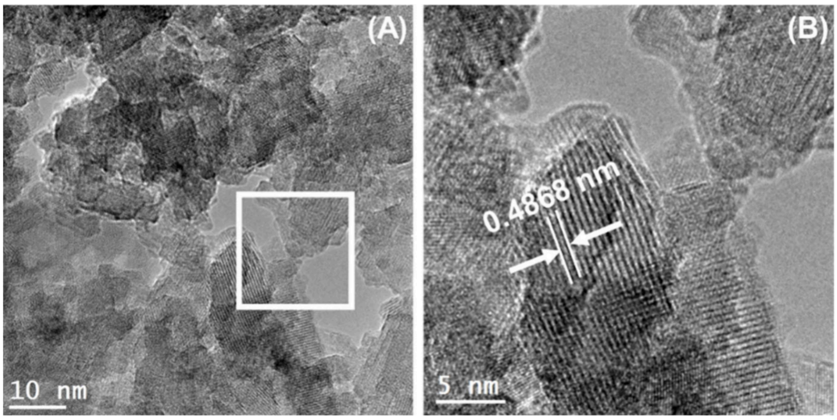

Figure 2. HRTEM images of 0.3 wt % Mn (Mn/Co = 0.011) promoted Co/γ-Al_2O_3 catalyst at 10 nm (A) and 5 nm (B) scale magnifications with *d*-spacing of 0.4868 nm.

electronic effects), as opposed to its migration to the support, in contrast to the case of TiO_2, where spinel phases were formed. Figure S5 shows the SAED patterns of the unpromoted, and 0.3, 3.1, and 7.5 wt % Mn (Mn/Co = 0–0.268) promoted Co/γ-Al_2O_3 catalysts with their corresponding *d*-spacings, which are attributed to the polycrystalline pattern of Al_2O_3 (Corundum, JCPDS-ICDD File No 46–1212),[82] the crystal phases of cobalt oxides,[75] and the phase of δ-MnO_2.[83]

3.2. Hydrogen Transient Isothermal Chemisorption (H_2-TIC) Followed by Temperature Programmed Desorption (H_2-TPD).

The dynamic rate profiles (μmol g^{-1} s^{-1}) of H_2 chemisorption at 100 °C obtained at the step gas switch He → 0.5% H_2/1% Kr/Ar/He (t) as a function of the Mn/Co molar ratio for the 20 wt % Co/x wt% Mn–Al_2O_3 (x = 0–7.5; Mn/Co = 0–0.268) catalysts are presented in Figure 3A.

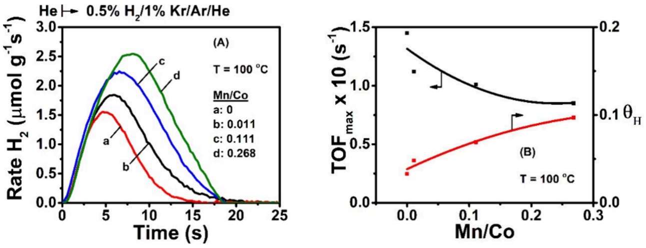

Figure 3. (A) Dynamic rates of H_2 adsorption (μmol g^{-1} s^{-1}) obtained after the step-gas switch He → 0.5% H_2/1% Kr/Ar/He (H_2-TIC) at 100 °C; (B) TOF_{max} (s^{-1}) and θ_H obtained after H_2-TIC as a function of Mn/Co molar ratio.

There is a clear increase in the total amount of chemisorbed hydrogen, N_H (μmol H g^{-1}), and a shift in the appearance of peak maximum with increasing Mn/Co ratio (t_{max} = 4.9, 5.9, 6.6, and 8.1 s). An increase in N_H by a factor of 1.6 was estimated after increasing the Mn/Co ratio from 0 to 0.268, and this is depicted in Figure 3B in terms of surface coverage, θ_H (based on the Co surface). It is important to mention that the largest θ_H estimated for the highest Mn loading (7.5 wt %) is only ~ 0.1; θ_H is expected to take values lower than 0.1 at 230 °C on a clean Co surface.

This increase in N_H cannot be linked to an increase in the exposed number of Co atoms with increasing Mn loading (Table 1, last column), where a decrease in the amount of surface Co by a factor of 1.2 was estimated. The fact that H_2 pretreatment of the catalysts at 425 °C for 2 h resulted in practically full reduction of cobalt oxide to metallic Co (see Section 2.1), a likely promoting effect of MnO_x toward reduction of any unreduced CoO_x at 100 °C (0.5% H_2/He gas mixture), the former being located on top of the Co particles or at the interface with the alumina support, must be excluded.

Morales et al.[14] reported an increase of H_2 chemisorption after increasing the Mn loading from 1.2 to 2.15 wt % but a decrease for higher Mn loadings in the case of Co/MnO-TiO_2. This behavior was explained by the spreading of MnO_x over the TiO_2 surface, which prevents SMSI between Co and TiO_2 (drop in H_2 chemisorption), while at higher Mn loadings, cobalt surface sites are covered by Mn, thus blocking H_2 chemisorption sites. The monotonic increase of H_2 chemisorption observed at 100 °C with increasing Mn/Co ratio on the present 20 wt % Co/MnO_x-Al_2O_3 catalytic system is suggested to be largely due to the increase of hydrogen chemisorption sites of similar energetics compared to the unpromoted Co/γ-Al_2O_3 but of different distribution, as evidenced by the H_2-TPD traces to be presented next. It should be mentioned that MnO_x/Al_2O_3 could also provide sites for H_2 chemisorption as reported elsewhere.[84]

It has been reported[85] that the effect of Mn loading on the Co reducibility depends on the catalyst synthesis method, where the amount of H_2 chemisorption increased with increasing Mn loading in the 0–7.5 wt % range. This behavior was attributed to two factors, namely, the prevention of cobalt particle agglomeration in the presence of MnO_x, and the decoration of the cobalt surface with manganese oxide nanoparticles/clusters, the latter being responsible for the enhanced reduction of cobalt oxide via electronic effects. Van Koppen et al.[86] reported that Mn acting as a structural promoter led to higher Co dispersions compared to the unpromoted catalyst. In the present 20 wt % Co/MnO_x-Al_2O_3 catalytic system, similar cobalt dispersions up to the Mn loading of 3.1 wt % (Mn/Co = 0.111), and a small decrease by ~ 17% of D_{Co}(%) after increasing the Mn loading to 7.5 wt % (Mn/Co = 0.268) were obtained (Table 1).

Figure 3B presents the effect of the Mn/Co ratio on the maximum value of the dynamic rate of hydrogen chemisorption at 100 °C (Figure 3A) in terms of turnover frequency (TOF_{max}, s^{-1}). The latter was estimated after using the total number of surface sites able to chemisorb hydrogen at 100 °C. It is evident that deposition of Mn onto the Co/γ-Al_2O_3 surface leads only to a small drop, ca. ~20–25%, in TOF_{max} when 0.3–7.5 wt % Mn (0.011–0.268 Mn/Co ratio) was deposited on the catalyst surface.

Figure S6A, B presents the effect of Mn/Co ratio on the H_2-TPD traces obtained following H_2 chemisorption at 100 °C (see Section 2.3). The variation of the Mn/Co ratio affects the number of hydrogen chemisorption sites with a given bonding strength on the cobalt surface (E_{Co-H}, kcal mol^{-1}), as revealed by the area under the desorption peaks. The total amount of hydrogen desorbed increased significantly with an increasing Mn/Co ratio (Figure S6C), in agreement with the results of Figure 3A. The amount of hydrogen desorption, N_H (μmol H g^{-1}) is equivalent to that of preadsorbed H in the 30–100 °C range, and this was found to be the lowest for the unpromoted catalyst, while it increased monotonically with the addition of Mn: 250, 310, 350, and 495 μmol H g^{-1} for 0, 0.011, 0.111, and 0.268 Mn/Co ratio, respectively. Additionally, the surface coverage of weakly bound H (T < 200 °C) was estimated to be larger compared to that of strongly bound H (T > 200 °C), and independent of Mn/Co ratio. An increase of Mn loading led to an increase in the concentration of Co sites capable of accommodating weakly bound H atoms. In fact, the maximum of the first H_2 desorption peak increases with increasing Mn/Co ratio, namely: 0.42, 0.55, 0.58, and 0.79 μmol H_2 g^{-1} s^{-1} for Mn/Co ratio of 0, 0.011, 0.111, and 0.268, respectively. It is shown in Figure S6C that when the amount of N_H is normalized to the total number of surface cobalt sites (Table 1), the equivalent θ_H is ~ 1.8 for the largest Mn/Co ratio used (ca. 0.268), while values of θ_H close to and smaller than unity were estimated for the unpromoted and Mn- promoted (Mn/Co = 0.011 and 0.111) Co/Al_2O_3 catalysts. This result along with the effect of Mn loading on the distribution of H-chemisorption sites (H_2-TPD traces), is consistent with the offered discussion regarding the H_2-TIC results (Figure 3A, B), where new hydrogen chemisorption sites of similar energetics toward H_2 chemisorption were formed (Co-MnO_x interfacial sites) in addition to those related to surface Co only. The

https://doi.org/10.1021/acscatal.4c07921
ACS Catal. 2025, 15, 5318–5338

possibility of H-spillover on the alumina surface should rather be excluded given the fact that N_H at 100 °C for the 7.5 wt % Mn (Mn/Co = 0.268) promoted catalyst corresponds to $\theta_H \sim 0.1$.

3.3. $^{12}CO/^{13}CO$ Isotopic Exchange at 155 °C.

3.3.1. Effect of Mn/Co Molar Ratio and H_2 Partial Pressure on θ_{CO}.

Figure 4A presents the influence of Mn/Co ratio on the dynamic evolution of the dimensionless concentration (Z) response curve of $^{13}CO(g)$ recorded during the step-gas switch 5 vol%^{12}CO/x vol% H_2/He → 5 vol% ^{13}CO/x vol% H_2/1 vol% Kr/Ar/He (t) at 155 °C in the absence of H_2 (x = 0), while Figure S7 presents similar results when 5 vol% H_2 was present in the CO/He feed gas stream. Figure 4B presents the effect of the Mn/Co ratio on the dynamic rate of ^{13}CO exchange (replacement of ^{12}CO-s for ^{13}CO-s). The largest Mn/Co ratio shows some small increase in the appearance of a shoulder after the time at which maximum exchange rate occurs (Figure 4B, d), suggesting the presence of some CO-s adsorption sites with slightly higher binding strength. The area under the R_{13CO} vs time curve (Figure 4B) determines the amount (μmol g^{-1}) and surface coverage of ^{12}CO-s exchanged for ^{13}CO-s (see Section 2.4), and results are reported in Figure 4C ($\theta_{^{13}CO}$) as a function of the H_2 concentration present in the CO/x vol% H_2/He adsorption gas mixture. In the case where no H_2 was present (CO/He feed gas stream), a clear increase in θ_{CO} by ~ 25% after increasing the Mn/Co ratio from 0 to 0.011 was obtained; a value of $\theta_{CO} \sim 0.28$ is noted. Further increases in the Mn/Co ratio to 0.111 and 0.268 had practically no effect on θ_{CO}. After introducing 5 vol% H_2 in the CO/H_2/He gas mixture, a significant increase in θ_{CO} for the Mn-promoted (Mn/Co = 0.011 and 0.111) Co/γ-Al_2O_3 catalysts was obtained, and less for the unpromoted catalyst (Figure 4C, a-c). The θ_{CO} appears to reach a maximum value for Mn/Co = 0.011 in the case of no hydrogen or 5 vol% H_2 present in the adsorption gas mixture. After the H_2 concentration was further increased to 10 vol%, the catalyst with Mn/Co = 0.111 exhibits the largest value of $\theta_{CO} \sim 0.45$ (Figure 4C, c). The increase in θ_{CO} when Mn was loaded in the Co/γ-Al_2O_3 catalyst suggests the formation of other specific CO chemisorption sites, like Co−O−Mn and/or Mn−O−Mn, in line with the HRTEM results (Section 3.1).

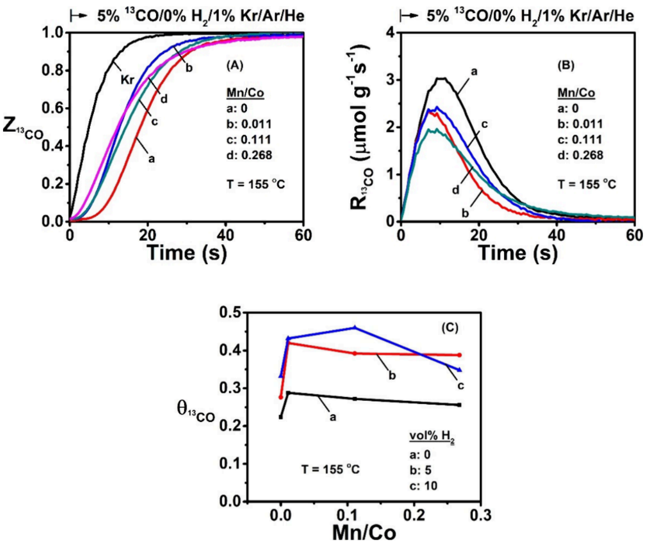

Figure 4. (A) Transient normalized concentration (Z) response curves of Kr and ^{13}CO obtained during the switch 5%^{12}CO/0% H_2/Ar/He (15 min) → 5%^{13}CO/0% H_2/1% Kr/Ar/He (t) at 155 °C as a function of Mn/Co ratio. (B) Dynamic rates of $^{13}CO(g)$ consumption as a function of Mn/Co ratio at 155 °C and in the absence of H_2 in the ^{13}CO adsorption gas mixture. (C) Surface coverage of exchangeable CO-s as a function of Mn/Co ratio and H_2 concentration (x = 0, 5, and 10 vol%) in the 5 vol% CO/x vol% H_2/He adsorption gas mixture.

The significant increase of θ_{CO} with increasing H_2 concentration in the CO/H_2/He gas mixture, independent of the Mn/Co molar ratio, requires some explanations. The effect of hydrogen concentration on the CO chemisorption on Co sites was investigated by Couble and Bianchi[87] over 10 wt % Co/γ-Al_2O_3 after applying the following sequence of step-gas concentration switches at 25 °C: He → 0.5% CO/x% H_2/He (x = 0 and 5) until equilibrium → He. The latter switches followed H_2 reduction (1 bar of H_2/440 °C) and cooling of the catalyst sample to 25 °C in H_2 gas flow. At the first switch, an overshoot in the H_2 concentration was seen, indicating the fast desorption of H-s from the surface in parallel to the CO adsorption, even in the use of H_2/CO ratio of 10. After purging with He (2nd switch), ~ 13% of chemisorbed CO was desorbed at 25 °C. These results suggested that competitive chemisorption between H_2 and CO at 25 °C is in favor of CO even under large H_2/CO gas ratios. This finding is supported by the results of the present work, where a low surface coverage of chemisorbed hydrogen ($\theta_H < 0.1$) was measured at 155 °C (Figure 3A, B). Thus, the significant increase of θ_{CO} estimated in the case H_2 is coadsorbed with CO must have a different origin of explanation.

The interaction of CO/H_2 with the −OH groups of the alumina support at 155 °C can give rise to the formation of formate species ($HCOO_s$) in a *reversible* step according to eq 11 as also mentioned in Section 2.4; a similar irreversible step could be applied.

$$CO(g)(\text{or } CO - s) + OH_s \leftrightarrow HCOO_s \tag{11}$$

We have probed for these reaction paths at 155 °C using *in situ* CO−DRIFTS, and the obtained results are presented in Figure S8A-B (SI). The recorded DRIFTS spectrum in the 1700−1300 cm^{-1} range on the catalyst with Mn/Co = 0.111 (largest θ_{CO}, Figure 4C, c) after 15 min in 5%^{12}CO/5 or 10% H_2/He, showed four IR bands at 1596, 1531, 1459, and 1380 cm^{-1} (Figure S8B). The IR bands at 1596 and 1380 cm^{-1} are due to the asymmetric and symmetric O−C−O stretching modes of HCOO (*formate*) species, while those at 1531 and 1459 cm^{-1} to *monodentate* and *ionic carbonate* species, respectively.[88] These IR bands due to formate and carbonates were also observed on bare alumina after treatment in 6.5% CO/He at 200 °C,[89] and on Co/Al_2O_3 after treatment in 1% CO/He at 265 °C.[87] The increase of H_2 concentration in the adsorption gas mixture from 5 to 10 vol% resulted in the increase of the intensity of all IR bands (Figure S8A). Also, similar but very weak IR bands (not shown) were recorded under 5%CO/He gas treatment. These results are in harmony with the work of Visconti et al.[90] who studied DRIFTS-CO chemisorption on Co/Al_2O_3 in CO/H_2 gas flow at room temperature.

A switch to the 5%^{13}CO/10%H_2/He gas mixture at the end of the gas treatment with 5%^{12}CO/10%H_2/He was then performed, and the DRIFTS spectrum was recorded after 15 min time-on-stream. We have observed a clear red shift of the IR bands at 1596 and 1380 cm^{-1} (under $^{12}CO/H_2$) to 1563 and 1360 cm^{-1} (under $^{13}CO/H_2$) following deconvolution (Figure S8B, C),[89] while no shift was identified for the two carbonate-types adsorbed species (1531/1459 cm^{-1}). In addition, part of the formate species did not provide the red isotopic shift, as illustrated in Figure S8C. These results can now provide strong evidence that the increase in the amount of consumed $^{13}CO(g)$ assigned to surface ^{13}CO-s (a small amount of produced $^{13}CO_2$ was subtracted) when H_2 was present in the CO adsorption gas (Figure 4C, b-c), compared to the case of CO/He (Figure 4C, a), is partly due to the equivalent amount of ^{13}CO participated in the reversible step of $H^{13}COO$-s formation (eq 11). Based on these results, it appears that the presence of H_2 in the CO adsorption gas mixture may have only a little effect on the adsorption of CO on the Mn-promoted cobalt surface.

In the case of use of the 5%CO/10%H_2/He gas mixture and for the Mn/Co = 0.111 catalyst, the amount of $^{12}CO(g)$ consumed after the switch He → $^{12}CO/H_2$/He (15 min) was equivalent to $\theta \sim 0.75$ (based on surface cobalt; CO_2 formation was subtracted), while that of $^{13}CO(g)$ consumed after the switch $^{12}CO/H_2$/He (15 min) → $^{13}CO/H_2$/He (t) was $\theta \sim 0.47$ (Figure 4C, c). Considering that the amount of reversible CO-s on the Mn-promoted cobalt surface was that estimated in the ^{13}CO/He isotopic experiment (no H_2 present; very small IR bands were seen), it was $\theta \sim 0.27$ (Figure 4C, a). The difference ($\theta \sim 0.2$) could then represent an upper limit for the surface coverage of the exchangeable HCOO species (eq 11). Based on these results, the surface coverage (upper limit) of the nonexchangeable formate species with $^{13}CO(g)$ would be $\theta \sim 0.28$.

3.3.2. Effect of Mn/Co Ratio on the Kinetic Rate Constant of CO-s Desorption.

The effect of the Mn/Co ratio on the specific rate constant of CO-s desorption (k_d, s^{-1}) studied in the $^{12}CO/^{13}CO$ isotopic exchange (Section 2.4) using the 5% CO/He gas mixture is presented in Figure 5. As we discussed in the previous section, the kinetic analysis of the transient $^{13}CO(g)$ response in the case when H_2 was present in the CO adsorption gas mixture must account for other surface reactions besides the CO adsorption on the supported cobalt surface, and this was out of the scope of the present work. Plots of $\ln(\theta_{CO})$ vs time for estimating k_d according to eq 4 are presented in Figure S9 for the unpromoted and Mn-promoted Co/γ-Al_2O_3 catalysts (Figure 4A). It is shown that as the Mn/Co ratio increases from 0 to 0.268, k_d drops by ~15%. Given the fact that $k_d = A_d \exp(-E_d/RT)$, and $E_d \sim \Delta H_{ads}$, the latter being proportional to the binding strength (E_b) of CO on the cobalt adsorption site, it appears that a small increase in the E_d and thus E_b with increasing Mn/Co ratio could explain the present behavior of k_d shown in Figure 5. The k_d dependence on the Mn/Co ratio (Figure 5) is in harmony also with the SSITKA-DRIFTS results (CO hydrogenation reaction at 230 °C) to be reported and discussed in Section 3.7.1, where a small red shift in the wavenumber corresponding to the C−O vibrational mode was recorded with increasing Mn/Co ratio.

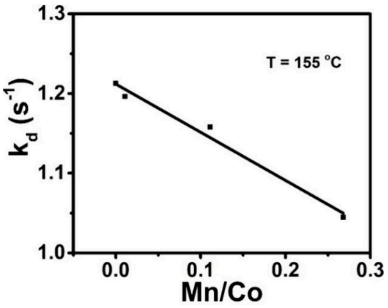

Figure 5. Kinetic rate constant of CO-s desorption, k_d (s^{-1}) at 155 °C as a function of the Mn/Co molar ratio (0−0.268). k_d parameter was estimated via eq 4 and based on the transient response curves of ^{13}CO recorded during the isotopic switch 5%^{12}CO/Ar/He → 5% ^{13}CO/1% Kr/Ar/He.

In a detailed study on the influence of Mn promotion on Co/SiO_2 catalyst, Johnson et al.[78] used *in situ* IR spectroscopy to show that Mn increases the amount of adsorbed CO but weakens the C−O bonding, thus strengthening the bonding of CO-s via the carbon atom on the Co° surface sites, suggesting increase of the activation energy for CO desorption and at the same time decrease of the corresponding rate constant, k_d. They suggested that this C−O bond weakening is enhanced by Lewis acid−base interactions between Mn^{2+} cations at the edges of MnO_x islands, which partly cover the Co nanoparticles, and the oxygen atom of adsorbed CO near this oxophilic component of MnO_x islands.

3.4. The Carbon Path of CO Hydrogenation to CH_4 as a Function of TOS-^{13}CO SSITKA/Mass Spectrometry.

The carbon path of CO hydrogenation reaction at 230 °C toward CH_4 formation for the Mn-promoted Co/γ-Al_2O_3 catalysts of varying Mn/Co molar ratio and time-on-stream, TOS (0.5, 2, 5, 10, 20, 30, 50 h) was investigated by ^{13}CO-SSITKA. Figure 6A shows the transient dimensionless concentration (Z) response curves for Kr (tracer gas), ^{13}CO and $^{13}CH_4$ recorded on the unpromoted Co/γ-Al_2O_3 catalyst at the switch $^{12}CO/H_2$/He (2 h) → $^{13}CO/H_2$/Kr/He (t). The transient response curve of $^{13}CO(g)$ lags behind that of Kr tracer due to the presence of reversibly adsorbed CO-s formed during the $^{12}CO/H_2$ reaction, while the transient response curve of $^{13}CH_4(g)$ lags behind that of $^{13}CO(g)$ due to the presence of a measurable quantity of *active* carbon-containing reaction intermediates (e.g., $-CH_xO$ and $-CH_x$). The position of $^{13}CH_4$ response curve relative to that of ^{13}CO depends on both the site activity (k, s^{-1}) of CH_xO/CH_x formation and hydrogenation to methane, and their surface coverages.[49] It is important to note that during the SSITKA switch, the sum of the dimensionless response curves of Z(^{13}CO) and Z(^{12}CO), and those of Z($^{13}CH_4$) and Z($^{12}CH_4$) should be equal to unity and cross each other at Z = 0.5. This important criterion that justifies the correct performance of SSITKA experiment was highly satisfied (Figure S10). Moreover, the concentration of

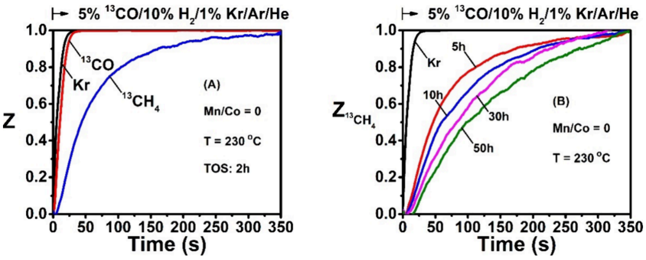

Figure 6. SSITKA normalized concentration (Z) response curves of (A) Kr, ^{13}CO and $^{13}CH_4$ after 2 h of CO hydrogenation, and (B) Kr and $^{13}CH_4$ after 5, 10, 30, and 50 h TOS in CO hydrogenation at 230 °C on the unpromoted 20 wt % Co/γ-Al_2O_3 catalyst.

H_2O remained stable during the SSITKA switch, underscoring again the accurate execution of the SSITKA experiments.[44]

As evidenced from Figure 6B, the time delay obtained between the $^{13}CH_4$ and Kr response curves over the unpromoted Co/γ-Al_2O_3 catalyst largely increases with increasing TOS, as opposed to the case of ^{13}CO response curve (Figure S11). This behavior is attributed to variations in the rate constant (k_{CHx}, s^{-1}) of hydrogenation of active $-CH_x$ species to CH_4 as well as to the decrease in θ_{CO} with TOS to be presented and discussed below.

Figure 7 presents the dynamic rates (μmol g^{-1} s^{-1}) of exchange of ^{12}CO-s for ^{13}CO-s and $^{12}CH_x$-s for $^{13}CH_x$-s which were estimated after 2 and 50 h of CO hydrogenation at 230 °C, following the ^{13}CO-SSITKA switch (eqs 6 and 7), as a function of Mn/Co molar ratio. The rate of CO-s exchange is notably higher than that of $-CH_x$, and the time required for the exchange of the total surface concentration of CO-s and active $-CH_x$ is ~40 and 250 s, respectively. The shape of the rate profiles for CO exchange at short TOS (ca. 2 h) appears similar for all Mn/Co ratios but different for the unpromoted 20%Co/γ-Al_2O_3 catalyst, where two peaks are discernible (Figure 7A). On the other hand, very similar shapes for the transient rates of CO-s exchange are seen for the unpromoted and Mn-promoted Co/γ-Al_2O_3 catalysts (Figure 7B). The shape of these transient exchange rates of CO-s largely reflect the kinetics of desorption of CO-s from the catalytic surface and thus the binding strength of M-CO (M: Co, Mn^{x+}) for the adsorbed surface structure present at a given TOS and CO hydrogenation reaction conditions. This is an important and very insightful information obtained by SSITKA and the rate analysis previously reported by us,[49] and *for the first time* over promoted Co-based CO hydrogenation catalysts. Integration of the R^{ex}_{CO} (t) curve provides the amount (μmol g^{-1}) and θ_{CO} under the applied CO hydrogenation reaction conditions.

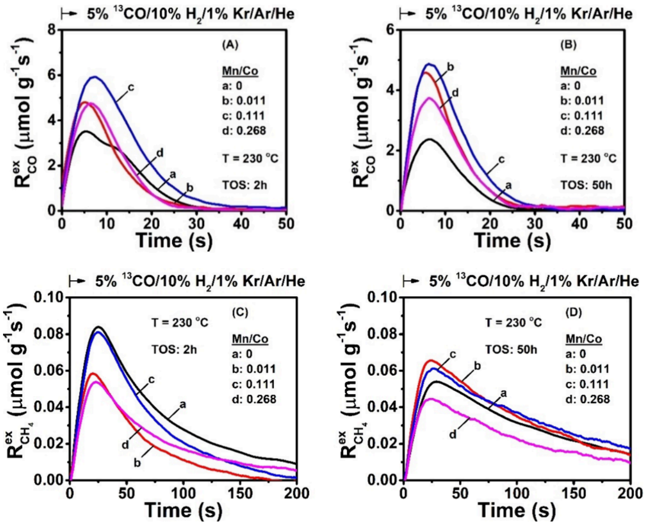

Figure 7. Dynamic rates (μmol g^{-1} s^{-1}) of (A, B) CO-s and (C, D) CH_x-s exchange obtained during the SSITKA switch 5% ^{12}CO/10% H_2/Ar/He (Δt_1) → 5% ^{13}CO/10% H_2/1% Kr/Ar/He(t) at 230 °C on the 20 wt % Co/MnO_x-Al_2O_3 (Mn/Co: 0, 0.011, 0.111 and 0.268) catalytic systems; Δt_1 = 2 and 50 h.

In the case of the dynamic rate of CH_x-s exchange, a large change in the shape of the rate response curve is observed when the TOS increased from 2 to 50 h (Figure 7C, D) irrespective of the Mn/Co ratio. There is a clear growth of the transient rate after the appearance of peak maximum (ca. 25 s, Figure 7D) compared to that developed during the initial period of the transient (ca. 0–50 s). Also, there is a slight but discernible shift in the time at which the peak maximum in R^{ex}_{CHx} (t) appears, and a clear decrease of its magnitude with increasing TOS (Figure 7C and D). As we have recently reported,[49] these characteristic features appearing in the R^{ex}_{CHx} (t) response provide strong support for the existence of *two types* of active C-containing species formed during CO hydrogenation at 230 °C with different activation energy for hydrogenation to CH_4 (E_{CHx}). The latter explains how the shoulder and tail appeared at larger times after the ^{13}CO-SSITKA switch. We have previously mentioned that hydrogenation of CO-s follows an H-assisted path, forming $-CH_xO$ and $-CH_x$ intermediates, subject to be further discussed in Section 3.7.2. Van Koppen et al.[86] reported that the C_1-selectivity increased at the expense of C_2–C_4 selectivity during prolonged TOS in FTS (220–240 °C, 20 bar) on Co–Pt/MnO-SiO_2 catalyst due to Mn mobility (migration from the Co metal onto the support), thus weakening the promotion effect. This phenomenon may also occur on the present catalysts of similar composition with that reported[78] and contributing to the effect of TOS on the dynamics of R_{CHx}(t) exchange.

The surface coverages (θ) of CO-s and CH_x-s as a function of the Mn/Co ratio and TOS are depicted in Figure 8A, C and B, D, respectively, and summarized in Table S1. It is shown that for long TOS, ca. 50 h, θ_{CO} is practically independent of the Mn/Co ratio (θ_{CO} ~ 0.2; Figure 8A, b). On the other hand, θ_{CHx} is maximum (θ_{CHx} ~ 0.025) but similar for the 0.011 and 0.111 Mn/Co ratios (Figure 8B, b). Also, similar θ_{CHx} values were obtained for the unpromoted and Mn/Co = 0.268 promoted catalysts for 2 and 50 h TOS, which appear lower by a factor of ~ 1.5 compared to the other two Mn/Co ratios of 0.011 and 0.111 in the case of 50 h TOS. Relatively large variations in θ_{CO} with TOS appear in all Mn-promoted Co/γ-Al_2O_3 catalysts except that of Mn/Co = 0.268 (Figure 8C, c). On the other hand, large variations in θ_{CHx} with TOS appear in all catalytic systems except for the unpromoted Co/

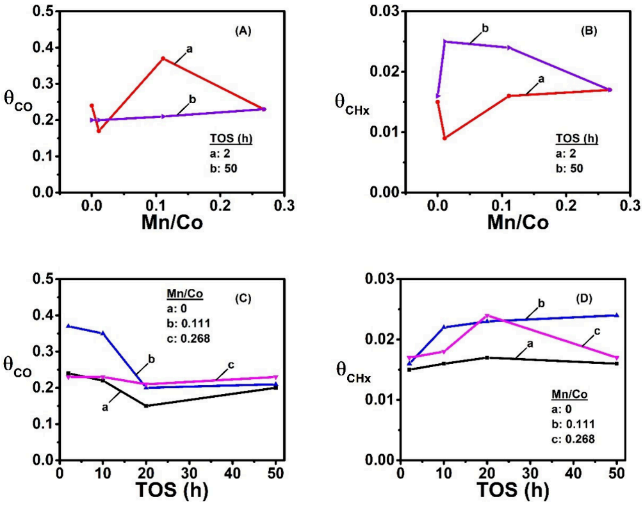

Figure 8. Surface coverage of reversibly adsorbed CO-s (A, C) and active CH_x-s (B, D) formed under the CO hydrogenation reaction at 230 °C (5%CO/10%H_2/He, 1.2 bar) as a function of TOS (h) and Mn/Co molar ratio.

γ-Al_2O_3 catalyst (Figure 8D, a). It is important to note that the surface coverages of CO-s and CH_x-s fall within the range of values reported elsewhere.[44,45,49,91−94] It appears interesting to note at this point that θ_{CO} values obtained at 155 °C after treatment of the catalysts with 5%CO/He for 15 min (Figure 4C, a) are of similar magnitude with those obtained under 5% CO/10%H_2/He at 230 °C and low CO-conversions and for long TOS (2−50 h). This implies that active CO chemisorption sites on the present Mn-promoted 20 wt % Co/γ-Al_2O_3 are only slightly influenced by the working composition of the adsorbed phase.

Den Breejen et al.[38] reported that on the 17 wt % Co-0.05 wt % Pt/Mn-SiO_2 FTS catalyst, after increasing the Mn/Co ratio from 0 to 0.25, the C_{5+}-selectivity increased due to the increased θ_{CHx} that favors an increased C−C coupling rate and chain-growth probability. In the present work, the 3.1 wt % Mn loading (Mn/Co = 0.111), which presented the largest value of θ_{CHx} for the largest TOS studied (ca. 50 h), also presents the largest chain-growth probability parameter (α=0.45) and effective rate constant for chain-growth (k^{g}_{eff}, s^{-1}) when compared to the other Mn/Co ratios, subject to be presented and discussed in Section 3.6. This observation aligns with findings reported by Vada et al.[91] who reported similar effects using LaO_x promoter on a 20 wt % Co/Al_2O_3 catalyst.

Table S1 reports the effect of the Mn/Co molar ratio and TOS in the CO hydrogenation reaction at 230 °C on the mean surface residence time of *active* CH_x (τ_{CHx}, s^{-1}) and that of molecularly adsorbed CO-s (τ_{CO}, s^{-1}). For long TOS (ca. 50 h), the latter appears rather independent of the Mn/Co ratio, as opposed to the case of τ_{CHx}, which varies in the 80−120 s range for a Mn/Co ratio in the 0−0.268 range. It was found that τ_{CHx} consistently increases with increasing TOS. On the other hand, variations in τ_{CHx} were observed with increasing Mn/Co ratio for a given TOS. For example, in the case of unpromoted and Mn/Co = 0.268 promoted Co/γ-Al_2O_3 catalysts, τ_{CHx} increased by 30 and 40%, respectively, when TOS increased from 30 min to 50 h. A notably larger increase (ca. ∼ 70%) was observed for the 3.1 and 0.3 wt % Mn loadings (Table S1).

Figure 9A, B shows the influence of Mn/Co ratio and TOS (ca. 2 and 50 h) on the TOF_{CH4} (s^{-1}) and k_{eff} (s^{-1}) for CH_4 formation, respectively. TOF_{CH4} was found to decrease with increasing TOS, while an increase with the Mn/Co ratio was evidenced up to the value of 0.111. The k_{eff} (s^{-1}) for CH_4 formation shows small changes with increasing Mn/Co ratio for long TOS (ca. 50 h), and a similar behavior except for Mn/Co = 0.011 and 0.111 was evidenced for short TOS (ca. 2 h, Figure 9B). For all Mn/Co ratios, k_{eff} exhibited significantly larger values for 2 h compared to 50 h TOS (Figure 9B and Table S1). This result suggests variation of either the intrinsic site activity for CH_4 formation (k) or θ_H with increasing TOS (k_{eff} = k θ_H). A novel methodology for decoupling the effect of an experimental condition (e.g., hydrogen partial pressure) on k and θ_H was recently reported by us.[49] This subject is outside the scope of this work.

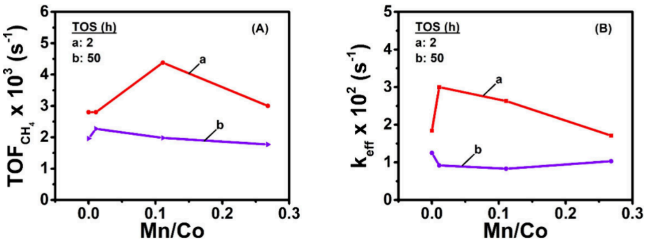

Figure 9. (A) TOF_{CH4} (s^{-1}) and (B) k_{eff} (s^{-1}) of the methane formation path as a function of TOS (ca. 2 and 50 h) and Mn/Co molar ratio.

Johnson et al.[78] examined the effect of variation of Mn/Co ratio in the 0.01−0.1 range on the TOF_{CH4} over a 10 wt % Co/Mn-SiO_2 catalyst. The TOF_{CH4} increased up to a Mn/Co ratio value of 0.1 but then decreased for larger Mn/Co ratio values. In the present work, the decrease in TOF_{CH4} with TOS could be attributed to the decrease in the intrinsic rate constant of CH_x hydrogenation (k_{CHx}), considering that an increasing Mn/Co ratio caused an increase in θ_H (Figure 3). As we previously reported,[49] the intrinsic site activity of $-CH_xO$ hydrogenation to CH_4 (k_{CHx}) was only slightly influenced by P_{H2}. The small influence was attributed to the effect of the surface concentration of coadsorbed carbonaceous and other oxygen-containing species (e.g., −OH) on the activation energy of CH_x-s hydrogenation, while θ_H was largely affected by the hydrogen pressure. Yang et al.[94] reported a TOF_{CH4} value of 2.3×10^{-3} s^{-1} on a 15 wt % Co/γ-Al_2O_3 catalyst at 210 °C, P_T = 1.8 bar, and a feed consisting of 3 vol% CO/30 vol% H_2/Ar. The obtained TOF_{CH4} compares well with that reported in Figure 9A and Table S1 ($2.0 - 2.8 \times 10^{-3}$ s^{-1}; TOS: 2−50 h) for the unsupported 20 wt % Co/γ-Al_2O_3 catalyst.

Theoretical analysis of the $^{12}CH_4$ normalized (Z) transient decay response curve obtained during the $^{12}CO/H_2 \rightarrow {}^{13}CO/H_2$ SSITKA switch (Figure S10) offers preliminary insights into the methanation process, according to the work of Bal'zhinimaev et al.,[95] Ledesma et al.,[54] and Shannon and Goodwin.[56] This analysis provides a first clue whether methanation proceeds via: (i) a single CH_x-s intermediate species (homogeneous pool), (ii) two chemically distinct CH_x-s intermediates in series (in the same path), or (iii) two chemically distinct CH_x-s intermediates participating in parallel carbon paths for the CH_4 formation. Each potential reaction path among those described above is characterized by profiles of ln(Z_{12CH4}) or ln(1-Z_{13CH4}) versus time of distinct features. Figure S12 presents plots of ln(1-Z_{13CH4}) vs time against the Mn/Co ratio after 50 h of CO hydrogenation reaction. Based on the observed delay in the decline of the ln(1-Z_{13CH4}) function and its concave downward shape, these features are characteristic of a two-pools in series model, each pool representing distinct in nature and activity reaction intermediate species. As we have shown in our recent publications,[49,53] the H-assisted CO hydrogenation mechanism for methane formation applies over the present unpromoted Co/γ-Al_2O_3 catalyst. In this mechanism, the first important intermediate, the −CHO (formyl) species, is further hydrogenated to $-CH_x$, with the latter leading to $CH_4(g)$ after further hydrogenation steps. As we will show later in Section 3.7.2, the same mechanism also applies over the Mn-promoted Co/γ-Al_2O_3 catalytic system. Based on the results of Figure S12, it appears that all four catalytic systems exhibit similar methanation reaction paths with some differences in the site activity (k, s^{-1}) and surface coverages for the two important $-CH_xO$ and $-CH_x$ intermediates. It is recalled at this point that the θ_{CHx} quantity estimated from SSITKA and presented in Figure 8B, D is the sum of the individual θ of $-CH_xO$ and $-CH_x$ active intermediates. It should be noted that curve c in Figure S12, which corresponds to the Mn/Co ratio of 0.111 (3.3 wt % Mn), lies above all the other curves. This feature implies that this catalyst composition exhibits the fastest $Z^{13}CH_4$ vs time transient response (see Figure 6B). The latter response is determined by the k and θ kinetic parameters associated with the two pools of active carbonaceous intermediates in series, as mentioned above.

According to the results of Figure 7D, the dynamic rate response of CH_x-s exchange shows a maximum at the initial 20 s of the transient, followed by a shoulder that extends out to more than 200 s and which is independent of the Mn/Co molar ratio. As previously discussed, these characteristic features probe the presence of two types of active carbonaceous intermediates, in harmony with the results of Figure S12.

3.5. Effects of Mn/Co Ratio and TOS on the Concentration and Reactivity toward H_2 of Carbonaceous Species Formed via CO Hydrogenation at 230 °C: TIH and TPH Studies.

Figure 10 presents the dynamic evolution of $^{12}CH_4$ and $^{13}CH_4$ formation rates (μmol g^{-1} s^{-1}) obtained during the transient isothermal hydrogenation (TIH) at 230 °C of carbonaceous species formed after CO hydrogenation at 230 °C followed by SSITKA, as a function of TOS (see Section 2.6) for the unpromoted and Mn/Co = 0.111 promoted Co/MnO_x-Al_2O_3 catalysts. The dynamic rate of $^{12}CH_4$ formation (Figure 10A, C) describes the kinetics of hydrogenation of inactive *^{12}C-containing* carbonaceous species, named C_β or "soft carbon",[45,46,49,88,96−98] which does not contribute to the formation of CH_4 under steady-state CO hydrogenation. These carbonaceous intermediates appear distinct in terms of structure and reactivity toward H_2 compared to the true *active* $-CH_x$ species (named C_α).[49] The time-on-stream (TOS) has a notable impact on the transient $^{12}CH_4$-rate shape for the unpromoted (0 wt % Mn) catalyst (Figure 10A) but only a small one for the 3.1 wt % Mn-promoted (Mn/Co = 0.111) catalyst (Figure 10C). Similar results were observed for the Mn-promoted Co/γ-Al_2O_3 catalysts of Mn/Co = 0.011 and 0.268.

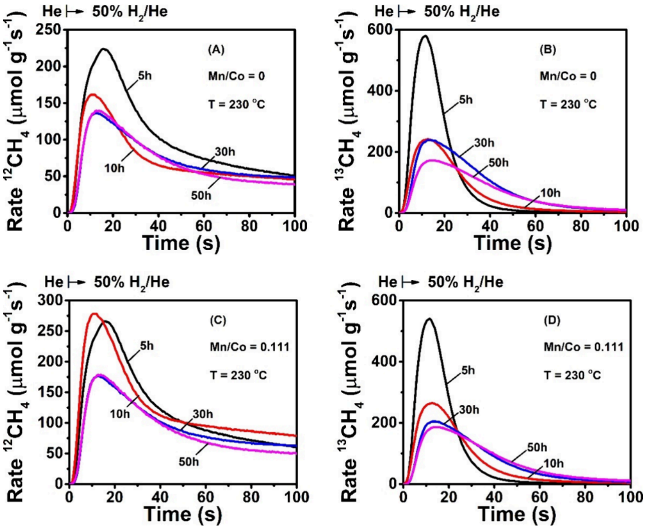

Figure 10. Transient hydrogenation rates of ^{12}C-containing species to $^{12}CH_4$ (A, C) and ^{13}C-containing species to $^{13}CH_4$ (B, D) obtained during TIH, following ^{13}CO-SSITKA for various times, Δt (h) in CO hydrogenation (5% ^{12}CO/10% H_2/Ar/He) at 230 °C over the unpromoted and 3.1 wt % Mn (Mn/Co = 0.111) promoted catalyst; Δt = 5, 10, 30, and 50 h.

Integration of the transient $^{12}CH_4$-rate curves provides the amount of C_β in terms of θ, and results are presented in Figure 11A, C as a function of Mn/Co ratio and TOS. It is evident that the quantity of C_β increases between short (2 h) and long TOS (50 h) irrespective of the Mn/Co ratio, while the largest quantity of C_β was observed for the 3.1 wt % Mn (Mn/Co = 0.111) promoted Co/γ-Al_2O_3 catalyst for all TOS (0.5−50 h; Figure 11C). The larger quantities of C_β obtained for higher Mn loadings, ca. 3.1 wt % (Mn/Co = 0.111) and 7.5 wt % (Mn/Co = 0.268) compared with the unpromoted catalyst is worth to be noted. The extended tail over 100 s observed in the transient rate of C_β hydrogenation to CH_4 regardless of the TOS should be noted. This feature aligns with findings from previous studies on Co/γ-Al_2O_3[44] and Rh/γ-Al_2O_3[88,89] catalysts. The extended tail is indicative of the formation of at least two types of C_β (different structure), and likely of different CO hydrogenation kinetics (RDS and/or E_{app}) to CH_4.

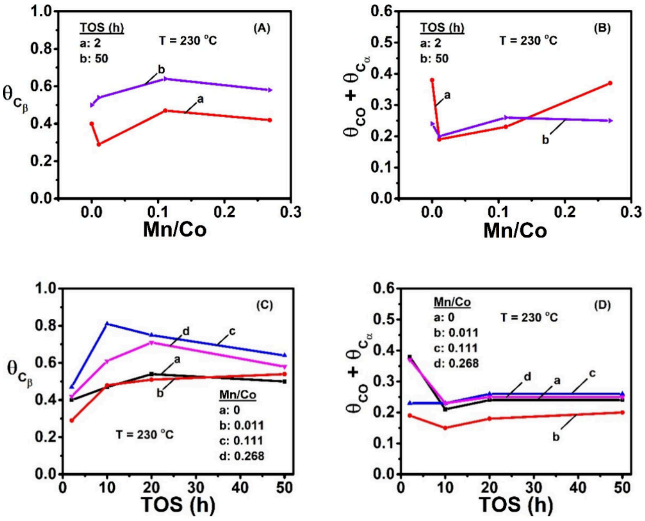

Figure 11. Surface coverage of nonexchangeable $^{12}C_\beta$ (A, C) and of the sum of active CH_x-s (C_α) and CO-s (B, D) determined after TIH (7 min) at 230 °C to $^{12}CH_4$ as a function of Mn/Co molar ratio and TOS (h).

Figure 10B, D presents the dynamic rate of $^{13}CH_4$ evolution attributed to the hydrogenation of ^{13}C-containing *active* reaction intermediates, CO-s and CH_x-s (named C_α), exchanged to ^{13}CO-s and $^{13}CH_x$-s at 230 °C (after the SSITKA switch), as a function of TOS for the unpromoted and 3.1 wt % Mn (Mn/Co = 0.111) - promoted Co/γ-Al_2O_3 catalysts. The sharp increase in the $^{13}CH_4$ rate within the first 5 s of the ransient is largely due to the hydrogenation of a small quantity of very active $-CH_x$ (C_α) species identified by SSITKA (Figure 8B, D). The subsequent response of the $^{13}CH_4$ rate, which is much faster than that of $^{12}CH_4$, results from the hydrogenation of ^{13}CO-s which was exchanged for ^{12}CO-s during SSITKA. The combined surface coverage (θ) of CO-s and C_α detailed in Table S1, differs by less than 10% when compared to that observed in Figure 11B, D for all Mn-promoted catalysts and TOS in CO hydrogenation. This small quantitative discrepancy is attributed to some desorption of ^{13}CO-s occurring during the 3 min He purge prior to the hydrogenation step.

Figure 12A presents the temperature-programmed hydrogenation (TPH) profiles of $^{12}CH_4$, following the ^{13}CO-SSITKA and the 7 min TIH steps as a function of TOS for

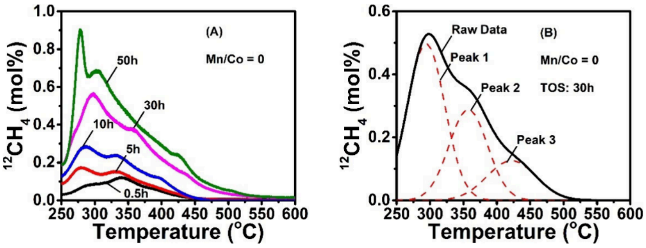

Figure 12. (A) Temperature-programmed hydrogenation (TPH) traces of ^{12}C-containing species to $^{12}CH_4$ after ^{13}CO-SSITKA for various times (Δt_1, h) in the CO hydrogenation reaction (5%^{12}CO/10%H_2/Ar/He) at 230 °C conducted on the unpromoted Co/γ-Al_2O_3 catalyst; Δt_1 = 0.5, 5, 10, 30, and 50 h. (B) Deconvolution of the TPH profile recorded after 30 h in CO hydrogenation at 230 °C.

the unpromoted Co/γ-Al_2O_3 catalyst. The deconvoluted $^{12}CH_4$-TPH trace after 30 h of the CO hydrogenation reaction at 230 °C is shown in Figure 12B, where three types of *inactive* carbonaceous species (named C_γ or "hard carbon") not hydrogenated at 230 °C were resolved. As presented in Figure 10A, C, the *inactive* C_β species consists of more than one type of carbonaceous species, likely of different chemical compositions and structure.

The equivalent surface coverage of C_γ as a function of the Mn/Co molar ratio and TOS in the CO hydrogenation reaction at 230 °C is presented in Figure 13. Notably, the amount of C_γ is significantly influenced by both the TOS and the Mn/Co ratio. For short TOS (ca. 2 h), the amount of C_γ is only slightly influenced by the Mn/Co ratio, as opposed to the case for 50 h. Additionally, based on the deconvoluted TPH profiles, like those of Figure 12B for Mn/Co = 0, a notably larger fraction of carbonaceous species was hydrogenated at lower temperatures with increasing TOS and Mn/Co ratio. The monotonic increase of C_γ with TOS for all Mn/Co ratios investigated is noted, where values of equivalent surface coverage, $\theta(C_\gamma)$ larger than 1.5 for TOS = 50 h for all Mn-promoted catalysts (Mn/Co = 0–0.268) was estimated. We have previously reported similar values for the unpromoted Co/γ-Al_2O_3 catalyst regarding the effect of Co particle size, H_2 pressure and TOS.[44,49,53] Also, SSITKA-DRIFTS studies reported by us[44] illustrated the formation of -C_xH_y adsorbed alkyl chains (x > 1).

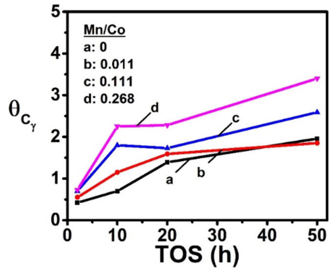

Figure 13. Surface coverage of inactive $^{12}C_xH_y$-s species (C_γ) hydrogenated to $^{12}CH_4$ in the 230–600 °C range (TPH) as a function of TOS and Mn/Co ratio (0–0.268).

At this point is important to note that after the SSITKA switch followed by the TIH/TPH runs, the catalyst was cooled in 50% H_2/He gas flow at 230 °C and the CO hydrogenation actvity ($^{12}CO/H_2$/He) was tested again. It was found that in all four catalysts tested (Mn/Co ratio: 0.0–0.268) and TOS (0.5–50 h), the catalytic activity measured was within 3% of the initial value for TOS lower than 10 h, and within 5% for TOS between 10 and 50 h. This result shows that structural changes of the fresh catalyst (reduced in H_2 at 425 °C/16 h) and loss of active catalytic sites even after 50 h TOS in the CO/H_2 reaction followed by TPH (up to 600 °C), seem to be small, if present.

In conclusion, a comprehensive investigation was conducted via the SSITKA technique followed by isothermal and temperature-programmed transient hydrogenation to unveil the influence of Mn/Co ratio and TOS in CO hydrogenation at 230 °C on the *active* C_α formed in the path of CH_4 formation, and the *inactive* C_β and C_γ carbonaceous species formed under low CO-conversions (X_{CO} < 20%). Possible intrinsic reasons for the influence of the Mn/Co ratio on the surface coverage of C_β and C_γ carbonaceous species will be given in the following Section 3.8.

3.6. Influence of Mn/Co Molar Ratio on the Chain-Growth and Hydrocarbon Selectivities of CO Hydrogenation at 230 °C (Kinetic Regime). The product distribution in terms of carbon-selectivity (S–C_n) for CH_4, C_2–C_5 hydrocarbons (sum of olefins and paraffins) and CO_2 products formation were measured under low-conversion (X_{CO} < 10%) to relate the obtained information with the various kinetic parameters estimated via the SSITKA technique followed by TIH/TPH experimental methodology. Thus, the S–C_n selectivities reported should be considered as *kinetic selectivities* related to the feed gas composition used (P_{CO} = 60 mbar, P_{H2} = 120 mbar and P_T = 1.2 bar). The CH_4-selectivity was found to decrease after the introduction of 0.3 wt % Mn (Mn/Co = 0.011) in the Co/γ-Al_2O_3, ca. 43% vs 54.3%, respectively (Table 2). Further increase of Mn loading to 3.1 wt % (Mn/Co = 0.111) and 7.5 wt % (Mn/Co = 0.268) led to a significant decrease of CH_4-selectivity, ca. 35.4% and 33.7%, respectively. The observed decrease in CH_4-selectivity with increasing Mn/Co ratio was also reported,[78,81] and this was attributed to the decrease in the ratio of surface coverage of adsorbed H-s to that of CO-s. In the present work, evidence was provided about the influence of the Mn/Co ratio on θ_{CO} for low CO conversions and for various TOS (SSITKA studies). In the case of TOS less than 10 h, θ_{CO} largely increased after increasing the Mn/Co ratio from 0 to 0.111 (Figure 8C). In addition, the amounts of *inactive* C_β and C_γ increased with increasing Mn/Co ratio (Figures 11C and 13), and this might reasonably lead to a decrease in the number of active sites, thus to θ_H. Therefore, similar conclusions to those reported[78,81] could be drawn from the present work that after increasing the Mn/Co molar ratio the θ_H/θ_{CO} ratio may decrease.

Table 2. CH_4, C_2–C_5 and CO_2 Product Selectivities and Chain-Growth Probability (α) after 5 h of CO Hydrogenation at 230 °C (P_T = 1.2 bar, P_{CO} = 60 mbar, H_2/CO = 2)

Catalyst (Mn/Co)	X_{CO} (%)	S_{CH4} (%)	S_{C2} (%)	S_{C3} (%)	S_{C4} (%)	S_{C5} (%)	S_{CO2} (%)	α
0	8.6	54.3	8.1	25.5	15.1	8.1	3.0	0.40
0.011	8.4	43.0	7.0	21.0	11.8	6.7	3.5	0.41
0.111	7.6	35.4	7.4	24.4	14.2	7.1	4.9	0.45
0.268	6.2	33.7	7.2	19.9	13.6	5.1	5.2	0.43

The kinetic selectivity values for C_{2+}-hydrocarbons reported in Table 2 were found to slightly depend on the Mn/Co ratio, which finds agreement with works reported at similar reaction conditions over the unpromoted and Mn-promoted Co/Al_2O_3 and Co/SiO_2 catalysts and of similar cobalt metal dispersion.[36,46,49,99−101] The chain-growth probability (α) was found to take the largest value in the case of Mn/Co = 0.111 (3.1 wt % Mn loading, Table 2); the chain-growth probability (α) dependence on Mn/Co ratio was estimated from linear plots of the respective product distribution for C_1 and C_3−C_5 hydrocarbons (combined paraffins and olefins) as depicted in Figure S13.[31] The increase in chain-growth parameter α after the addition of Mn promoter to Co/SiO_2 was also reported for the CO hydrogenation at 215 °C and $P_T = 1$ or 10 atm ($P_{CO} =$ 372 mbar, $H_2/CO = 2$).[36] This was attributed to a reduction in the intrinsic rate of chain termination through the hydrogenation of surface carbon to methane. Moreover, Weckhuysen and his group[14] reported a continuous decrease of S_{CH4}(%) with increasing Mn/Co ratio (0−0.45) and a concomitant enhancement in C_{5+}-selectivity over the 8 wt % Co/MnO-TiO_2 catalytic system for the CO hydrogenation at 220 °C and 1 bar total pressure. At the same time, an optimum Mn/Co ratio of 0.31 (2.15 wt % Co) was reported for maximum activity (mol CO gCo^{-1} s^{-1}). The authors concluded that MnO_x species elicit both structural and electronic promotional effects, which resulted in an improved cobalt dispersion but a CO hydrogenation activity at intermediate Mn loadings. In the present work, the slight increase in CO_2 selectivity (∼2%-units) with the introduction of Mn (Table 2) might be attributed to the occurrence of the reverse water−gas shift (RWGS) reaction on the surface of MnO_x clusters/particles.[102−105]

DFT calculations performed on modeled MnO_x clusters placed on the Co(111) surface revealed that Mn promotion is associated with improved oxygen removal from the active catalytic surface, explaining the decreased CO_2 and CH_4 selectivity.[13] Johnson et al.[78] based on a H-assisted CO hydrogenation path for FTS, and a relevant kinetic rate expression, reported that the higher CO equilibrium adsorption constant (K_{CO}, L-H isotherm), and the increased apparent rate constant k for adsorption, correlate with a reduction in methane production and an increase in the C_{5+}-hydrocarbons selectivity after Mn was introduced in the 10 wt % Co/SiO_2 catalyst. The increased θ_{CO} observed due to the formation of new adsorption/catalytic sites on the Mn-promoted surface along with the enhanced CO dissociation obtained were qualitatively consistent with reduced hydrogen availability. This in turn favored chain growth over methanation and hydrogenation termination reactions.[78]

According to the H-assisted CO dissociation path,[49,53] the $-CH_x$ intermediates could be converted either to CH_4 or to higher hydrocarbons, C_{2+}, thus acting as a chain initiator.[94] We have applied the kinetic analysis proposed by Yang et al.[94] to estimate the effective rate constant for chain growth, $k_{eff}^{g}(s^{-1})$, according to the following relationship:

$$k_{eff}^{g} = k_{eff}^{CH4}(Rg/R_{CH4}) \tag{12}$$

where k_{eff}^{CH4} is the effective rate constant for methane formation, which is estimated from the SSITKA analysis (Section 3.4, Figure 9C, Table S1), R_{CH4} is the kinetic rate of methane formation (Table S1), and R_g (μmol C g^{-1} s^{-1}) is the chain-growth rate of $-CH_x$ estimated via a material balance (eq 13):

$$R_g = R_{CO} - R_{CH4} \tag{13}$$

In eq 13, R_{CO} is the kinetic rate of the conversion of CO (μmol C g^{-1} s^{-1}) into hydrocarbons and CO_2 gas products.

Figure 14 illustrates the effect of the Mn/Co ratio on the k_{eff}^{g} of the CO hydrogenation at 230 °C and after long TOS (ca. 50 h). It is seen that there is an optimum Mn/Co ratio or wt % Mn loading for which chain-growth site activity (average) is maximum. The observed value of Mn/Co = 0.111 or 3.3 wt % Mn loading is in line with the largest chain-growth parameter α, previously reported and discussed (Table 2). The present SSITKA work of CO hydrogenation showcased that important catalyst composition design parameters can be tailored to mimic industrial FTS reaction performance. As stated earlier, a very similar Mn/Co ratio was found to be optimal for the industrial production of sustainable aviation fuels on a Co-based industrial FTS catalyst.[40]

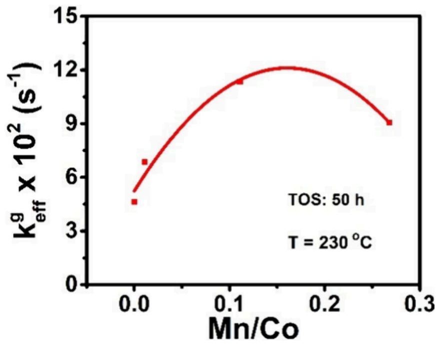

Figure 14. Effect of Mn/Co molar ratio (0 − 0.268) on the effective rate constant, k_{eff}^{g}, of chain-growth for the CO hydrogenation reaction at 230 °C over the 20 wt % Co/MnO_x-Al_2O_3 catalytic system and after 50 h TOS.

3.7. In Situ DRIFTS. *3.7.1. SSITKA-DRIFTS.* SSITKA-DRIFTS experiments were conducted following the step-gas switch $5\%^{12}CO/10\%H_2/Ar$ (230 °C, 2 h) → $5\%^{13}CO/10\%$ H_2/Ar (t), aiming to reveal the influence of the Mn/Co molar ratio on the reactivity of different types of adsorbed CO-s formed on the 20 wt % Co/x wt % Mn−Al_2O_3 catalysts. Figure 15A displays the recorded IR bands within the CO-IR region (1800−2250 cm^{-1}) and their subsequent deconvolution into five distinct IR bands before and after the SSITKA switch for the Mn-promoted (Mn/Co = 0.111) Co/MnO_x-Al_2O_3 catalyst. IR bands marked 1 and 2 refer to the R and Q branches of

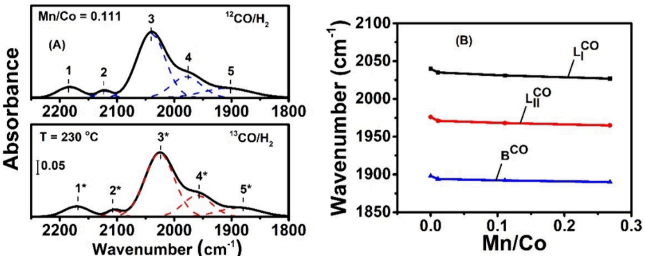

Figure 15. (A) SSITKA-DRIFTS spectra recorded in the CO IR-region (2200−1800 cm^{-1}) before (2 h in $^{12}CO/H_2$) and after 10 min of the SSITKA switch at 230 °C on the Mn promoted (Mn/Co = 0.111) Co/γ-Al_2O_3 catalyst; (B) Peak center of IR bands (cm^{-1}) for the three types of adsorbed CO-s (determined after deconvolution) as a function of Mn/Co molar ratio.

gaseous CO, while IR bands marked 3, 4, and 5 refer to adsorbed CO-s species.[14,60,106,107] Notably, the application of the SSITKA switch led to a red isotopic shift (ca. 30−40 cm^{-1} after deconvolution) in all five IR bands. This shift indicates that the three types of adsorbed CO-s are reversibly chemisorbed onto the cobalt surface, in agreement with the SSITKA-Mass Spectrometry findings reported in Figures 6A and 7A, B. However, the participation of all three types of adsorbed CO-s in the formation of $-CH_x$ precursor species for methane and higher hydrocarbons cannot be confirmed based on the appearance of the red isotopic shift only. On the other hand, it should be pointed out that at least one of these types of CO-s must be considered as precursor to all the derived hydrocarbon products. In terms of chemical structure, the three identified types of CO-s are assigned to linear CO-s and bridged-type CO-s associated with distinct Co surface sites, namely: surface defects, on-top hollow, and 3-fold hollow sites.[49,108−110] In the case of unpromoted Co/γ-Al_2O_3 catalyst, the IR bands associated with CO-s consisted of an IR band centered at 2040 cm^{-1} and assigned to a HF-linear CO-s, an IR band at 1976 cm^{-1} assigned to a LF-linear CO-s, and an IR band at 1900 cm^{-1} assigned to a bridged-type CO-s.[108]

By observing the trend of the IR band position with increasing Mn/Co ratio or Mn loading (Figure 15B), it is shown that all three IR bands of CO-s experienced a red shift toward lower wavenumbers. For instance, when Co/γ-Al_2O_3 is promoted with 7.5 wt % Mn (Mn/Co = 0.268), the CO-s IR bands shifted to 2027 (2040), 1965 (1976), and 1890 (1900) cm^{-1}; numbers in parentheses correspond to the case of Mn/Co = 0. This shift might be indicative of an increase in the binding strength (kJ mol^{-1}) of CO with the Co surface, E_b (Co_s-CO). On the other hand, the effect of θ_{CO} on E_b should be also examined. According to the SSITKA results of Figure 8A, a, θ_{CO} increases with increasing Mn/Co ratio; thus, a lowering of the binding strength and a blue shift in the IR band of CO-s would be expected. It is therefore reasonable to suggest that the small red shift in the position of the IR bands of the CO-s in the CO hydrogenation reaction at 230 °C with increasing the Mn/Co ratio is due to some strengthening of the E_b (Co_s-CO).

Johnson et al.[78] conducted an extensive study on a series of Mn-promoted Co/SiO_2 catalysts. They reported that the HF-linear CO-s experienced a red shift of up to 9 cm^{-1} when the Co/Mn ratio was increased to 0.5 compared to that of the unpromoted counterpart. This red shift was attributed to the formation of under-coordinated Co atoms in the presence of MnO_x deposited on the cobalt surface, which led to CO-s with weakened carbonyl bonds. Furthermore, Morales et al.[14] identified the formation of two linear type CO-s species formed on the Mn-promoted Co/TiO_2. They found that an increase in Mn content led to a relatively higher concentration of LF-linear CO-s compared with the HF-linear CO-s counterpart. This behavior was linked to the MnO_x promoter's ability to withdraw electron density from the Co, which in turn reduces π^* back-donation to the adsorbed CO-s, thus increasing the carbonyl stretching frequency and weakening the C−O bond strength. The latter corresponds to the enhancement of CO dissociation.[38,39,111] The latter finds strong support by the present transient kinetics of the hydrogenation of CO-s (using DRIFTS) results that follow.

3.7.2. Transient Kinetics of CO-s Hydrogenation: DRIFTS Study.

The influence of the Mn/Co ratio on the kinetics of hydrogenation of the individual types of adsorbed CO-s formed under the CO hydrogenation reaction at 230 °C was investigated by transient isothermal hydrogenation conducted in the DRIFTS reactor cell. Following CO hydrogenation (5% CO/10% H_2/Ar) at 230 °C/2 h and a 3 min 1%Kr/Ar purge, a step-gas switch to 50 vol %H_2/Ar gas mixture was made. During the latter switch, the transient decay response curves of Kr and CO measured by a mass spectrometer (*operando* DRIFTS-MS) were practically identical for all catalysts investigated, confirming the fact that the rate of CO desorption during hydrogenation of CO-s was negligible. This result was also reported previously.[49,53]

Figure S14A shows the DRIFTS spectra recorded in the 1800−2200 cm^{-1} IR region for the transient hydrogenation of adsorbed CO-s formed over the unpromoted Co/γ-Al_2O_3 catalyst. The spectrum labeled as ″Ar (0 s)″ corresponds to the state after the 3 min Ar purge of the reactor cell. The spectrum labeled ″H_2/Ar (t)″ corresponds to the time, t, in the 50% H_2/Ar hydrogenation gas mixture. As time progresses during the hydrogenation process, θ_{CO} gradually decreases, and this is accompanied by a corresponding shift of the associated IR band toward lower wavenumbers. This red shift is largely attributed to the influence of θ_{CO} (lateral repulsive interactions) on the binding energy of adsorbed CO-s. Additionally, the presence of coadsorbed $-CH_x$ and other carbonaceous species might also have an impact on the binding strength of CO-s on the cobalt surface.

The microkinetic analysis of the transient isothermal hydrogenation process for each type of adsorbed CO-s was conducted using the deconvoluted DRIFTS-TIH spectrum shown in Figure S14B after 3 min of Ar purge and just before the switch to the 50%H_2/Ar gas mixture. The same deconvolution procedure was applied for the spectra recorded during hydrogenation in 50%H_2/Ar for all of the other catalysts. A significant part of the adsorbed CO-s was converted to $CH_4(g)$ within the first 3 min of hydrogenation (Figure S14A). Figure S15A, B displays linear plots of ln[α] against the time of hydrogenation of the L_I and L_{II} linear type adsorbed CO-s, respectively, as a function of Mn/Co ratio, according to the kinetic modeling and analysis reported by us.[49,53] The α parameter appeared in eq 14 is defined as follows:[49]

$$\ln[a] = -k_{eff}t; \qquad a = A_{CO}(t)/A_{CO}(t = 0) \tag{14}$$

A_{CO}(t) and A_{CO}(t = 0) are the integral IR band intensities for each linear-type adsorbed CO-s at a given time, t, and t = 0 (before the H_2/Ar switch), respectively; these quantities are considered proportional to the surface coverage of the CO-s. Due to the small integral band area of the bridged-type (B) adsorbed CO-s, a similar analysis related to this species was not attempted. By using eq 14, the slope of the linear plot ln[α] versus time provides the apparent rate constant (k_{eff}) of the hydrogenation to $CH_4(g)$ of the linear-type adsorbed CO-s.[49,53] The estimated k_{eff} values for both linear-type CO-s species as a function of the Mn/Co ratio are presented in Figure 16A. The k_{eff} values obtained align with the range of values previously reported over different Co/γ-Al_2O_3 catalysts at 200 and 230 °C and other CO hydrogenation reaction conditions.[45,49,53] It is shown that the L_I and L_{II} adsorbed CO-s species exhibit the largest value at a different Mn/Co ratio, namely, 0.011 and 0.111, respectively. However, the ratio of k_{LI}/k_{LII} (intrinsic rate constants) for the HF-linear to that of LF-linear CO-s varies with the Mn/Co ratio as depicted in Figure 16B; it should be noted that k_{eff} = k θ_H. For the

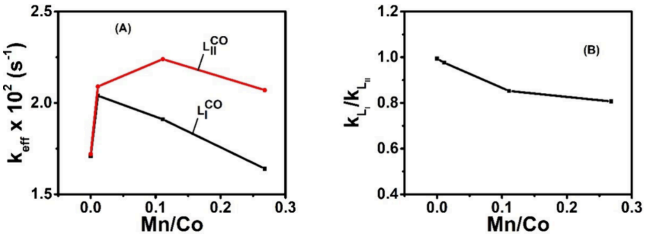

Figure 16. (A) Apparent kinetic rate constant (k_{eff}) of the RDS of hydrogenation to CH_4 of L_I and L_{II} adsorbed CO-s species formed after 2 h of CO hydrogenation at 230 °C as a function of the Mn/Co molar ratio. (B) Ratio of the intrinsic kinetic rate constants of the hydrogenation to CH_4 of the L_I and L_{II} CO-s species.

unpromoted Co/γ-Al_2O_3 catalyst, k_{eff_LI} = 0.0170 s^{-1} and k_{eff_LII} = 0.0172 s^{-1}, resulting in k_{LI}/k_{LII} ~ 0.98. On the other hand, for the 7.5 wt % Mn-promoted catalyst (Mn/Co = 0.268), a value of k_{LI}/k_{LII} ~ 0.80 was estimated.

The decrease in the relative site activity of the RDS of CO-s hydrogenation suggests that an increased concentration of MnO_x incorporated in the Co/γ-Al_2O_3 catalytic surface might enhance the withdrawal of electrons from the Co surface, leading to a reduction in the antibonding π^* back-donation to adsorbed CO, thus weakening of the C−O bond strength in s-C═O species, which in turn facilitate the −CHO and $-CH_x$ formation. The latter in conjunction with the θ_H is expected to govern the rates of chain-growth steps (C_{2+}-hydrocarbons formation) against methanation reaction steps. Given the fact that the surface coverage of L_I^{CO} appears larger than that of L_{II}^{CO} (Figure S14B), the importance of CO hydrogenation via CH_xO-s/CH_x-s intermediates formation and chain growth (α) must be focused on the HF-linear CO-s (L_I^{CO}) via the *chemical nature* of adsorption sites. This fundamental information gathered from the present transient isothermal hydrogenation of individual adsorbed CO-s via DRIFTS could pave the way for the design of Mn-promoted Co surfaces with optimum higher-hydrocarbon yields.

3.8. An Overview of the Effect of Mn on Important Kinetic Parameters of CO Hydrogenation at 230 °C over the 20 wt % Co/MnO_x-Al_2O_3 Industrially Relevant Catalyst.

Given the absence of visible MnO_x nanoparticles at the lowest Mn promoter loading used (0.3 wt %, Mn/Co = 0.011) but its clear effects on SSITKA, H_2 and CO chemisorption, it is reasonable to consider the good dispersion of MnO_x clusters (overlayer) resulting in a considerable fraction of surface Co being in contact with the Mn promoter (Scheme 1, right). As the Mn loading increases to 3.1 and 7.5 wt %, larger segregated MnO_x particles are formed on the γ-Al_2O_3 support and at the interface with the Co particles, while larger enriched regions of the Co surface with MnO_x could be envisioned according to the EDX spectra shown in Figure 1 (Scheme 1, left).

Dynamic H_2 chemisorption at 100 °C followed by TPD revealed that new hydrogen chemisorption sites of similar energetics were formed upon the addition of the Mn promoter onto the surface of Co/γ-Al_2O_3, the concentration of which was monotonically increased along with the fraction of weakly bound H-s. These results revealed the importance of θ_H at 230 °C in controlling the chain growth ($-CH_x$ coupling) against the methanation reaction (hydrogenation of $-CH_xO$ and $-CH_x$ species). The latter was recently highlighted by Zhu et al.[32] in the case of Co-MnO_x/SiO_2 for justifying the significant enhancement in the yield of C_{2+} olefins and olefins/paraffins ratio in FTS. In the present work, the Mn/Co molar ratio influenced to a small extent the binding strength of adsorbed CO-s under CO hydrogenation reaction conditions, but to a larger extent the reactivity of the two identified linear type adsorbed CO-s (HF-L_I^{CO} and LF-L_{II}^{CO}) toward CH_4 formation. The relative methanation activity of L_I^{CO} to that of L_{II}^{CO} in terms of the specific kinetic rate constant (k_{LI}/k_{LII}) was found to constantly decrease with increasing Mn/Co ratio from 0 to 0.268 (0 to 7.5 wt % Mn), where k_{LI} for the HF-L_{CO} was about 25% lower than k_{LII} for the LF-L_{CO}. For large TOS (ca. 50 h), θ_{CO} increases to a small extent but θ_{CHx} passes through a maximum with increasing Mn/Co molar ratio. CH_4 kinetic selectivity decreases with increasing Mn/Co ratio. This was suggested to be due to a likely lower θ_H/θ_{CO} ratio on the catalyst surface.

Scheme 1. Visualized Interface between Co Nanoparticles (10−12 nm) and MnO_x as a Function of Mn/Co Molar Ratio (0.011−0.268) or Mn Loading (0.3−7.5 wt %) for the 20 wt % Co/MnO_x-Al_2O_3 Industrially Relevant Catalytic System

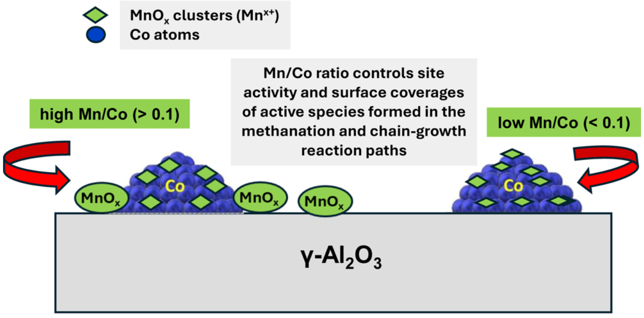

The chain-growth parameter (α) and the apparent rate constant, k_{eff}^g for chain-growth were found to pass through a maximum in the 0−0.268 Mn/Co range, at Mn/Co of 0.111 (3.1 wt % Mn). This result is consistent with the largest θ_{CHx} value measured by SSITKA after 50 h TOS. These experimental findings of the influence of Mn/Co ratio on important kinetic and chemisorption parameters of CO hydrogenation at 230 °C over the Mn-promoted Co/γ-Al_2O_3 catalytic system strongly relates to the structural state of Mn promotion depicted in Scheme 1. The concentration and local chemical environment of interfacial sites (e.g., Mn−O−Co) alter the electronic structure of Co and create new chemisorption sites for H_2 and CO. This becomes important for the rate control of H_2 and CO chemisorption/dissociation, and further hydrogenation of CO-s to $-CH_xO$ intermediates, as evidenced in the present work. A balance between unpromoted and Mn-promoted cobalt surface sites appears to control the dependence of the kinetic parameter k_{eff}^g for the chain-growth of $-CH_x$ intermediates to higher hydrocarbons on Mn/Co molar ratio (Figure 14).

The extent of formation of *inactive* -C_xH_y adsorbed alkyl hydrocarbon species, C_β, "soft carbon", and C_γ, "hard carbon", and their activity toward hydrogen (50% H_2/He) were largely affected by the Mn/Co ratio and TOS (ca. 2−50 h). Unpromoted (Mn/Co = 0) and Mn-promoted Co/γ-Al_2O_3 of low Mn loading (0.3 wt % Mn; Mn/Co = 0.011) provided the lowest amounts of C_β and C_γ for all TOS (ca. 2−50 h) investigated, while significantly larger amounts, ca. 0.5−2.5 times were estimated for the higher Mn/Co ratios. For long

TOS (ca. 50 h), larger amounts by 10−20% of C_β and C_γ were measured for Mn/Co = 0.111 compared to the other Mn loadings. This was found not to influence the optimum values of the related kinetic parameters of chain-growth for this catalyst composition (20 wt % Co/3.1 wt % Mn-Al_2O_3. This is another important result of this investigation, which highlights the control imposed by the Mn/Co ratio on the occupation of surface sites by inactive carbonaceous species not relevant to the carbon paths of chain growth.

4. CONCLUSION

By combining ^{13}CO-SSITKA followed by transient isothermal and temperature-programmed hydrogenation experiments, the influence of Mn/Co molar ratio (0−0.268) on the composition (surface coverage) and activity of the working adsorbed phase (active and inactive carbonaceous species) during CO hydrogenation at 230 °C (total P = 1.2 bar) over the 20 wt % Co/MnO_x-Al_2O_3 catalytic system was determined for the first time to the best of our knowledge. High-Resolution Transmission Electron Microscopy (HRTEM) and elemental mapping (EDX) revealed that addition of Mn in the catalyst formulation (0.3 to 7.5 wt % or Mn/Co ratio in the 0.011−0.268 range) displayed diverse MnO_x-Co structural configurations. MnO_x was found to either surround Co nanoparticles or chemically interact with them. The increase in the Mn/Co molar ratio led to the formation of Co-MnO_x agglomerates. These structural changes only slightly altered the cobalt mean particle size, ca. 10.5−13.0 nm. The role of the Mn promoter was therefore largely electronic due to the intimate contact established between MnO_x clusters and Co nanoparticles, suggesting that sites along the interface were responsible for the promotion effect. A balance between unpromoted and Mn-promoted cobalt surface sites appears to well explain the dependence of the kinetic parameter k^g_{eff} for chain-growth on the Mn/Co molar ratio.

An increased concentration of active sites for H_2 chemisorption at 100 °C with an increasing Mn/Co ratio was evident in the Mn-promoted Co/γ-Al_2O_3 catalytic system, also affecting the distribution of the H-binding states. The ^{12}CO/^{13}CO isotopic exchange at 155 °C (5 vol % CO/He) indicated only a small enhancement of CO chemisorption with increasing Mn/Co ratio. On the other hand, when 5 or 10 vol % H_2 was present in the 5%CO/He adsorption gas, a considerable concentration of HCOO (formate) species was formed ($\theta \sim 0.2$−0.4), practically independent of Mn/Co ratio. Kinetic analysis of the dynamics of ^{12}CO/^{13}CO exchange (CO/He) at 155 °C showed that the rate constant for CO-s desorption (k_{des}) decreased with increasing Mn/Co ratio; a decrease by ∼15% was noticed after increasing the Mn/Co from zero to 0.268. ^{13}CO-SSITKA-DRIFTS revealed the presence of two linear type and one bridged type adsorbed CO species populated under CO hydrogenation at 230 °C. Slightly weakened CO stretching energies in comparison to the unpromoted catalyst was found. Additionally, larger surface coverages of HF-L_I^{CO} compared to LF-L_{II}^{CO} were obtained, while the rate constant (k, s^{-1}) of the RDS of the hydrogenation of CO-s to methane was found to be smaller for L_I^{CO} compared to that of L_{II}^{CO}. The ratio of k's for the L_I^{CO} and L_{II}^{CO} was found to decrease by ∼20% when the Mn/Co ratio increased from 0 to 0.268 (0 to 7.5 wt % Mn).

^{13}CO-SSITKA studies revealed that the dynamic net rate of CO adsorption and that of $-CH_x$ formation were largely influenced by the Mn/Co ratio. It was illustrated that these dynamic rates significantly influenced the θ_{CO} and θ_{CHx} (active species for CH_4 formation) kinetic parameters with time-on-stream in CO hydrogenation. For long TOS (ca. 50 h), θ_{CO} and θ_{CHx} values at Mn/Co of 0.111 (Mn loading at 3.1 wt %) justify the largest values of chain growth parameter (α) and effective kinetic rate constant, k^g_{eff} obtained when compared with the other Mn/Co ratios investigated. The higher Mn/Co ratios used (0.111 and 0.268) caused an increase in the accumulation of *inactive* ″soft carbon″ (C_β) and ″hard carbon″ (C_γ) with increasing TOS compared to the unpromoted catalyst. For long TOS (ca. 50 h), the 10−20% larger amounts of C_β and C_γ formed in the case of Mn/Co = 0.111 when compared with the other Mn/Co ratios did not affect its optimum catalytic performance (at low CO conversions) in terms of chain growth parameter, α.

Conclusively, the present work provided deep insight about the influence of Mn incorporation (0.3−7.5 wt %; Mn/Co ratio between 0.011 and 0.268) in the 20 wt % Co/γ-Al_2O_3 industrially relevant catalytic system on important kinetic parameters of the carbon paths of methanation and chain-growth in CO hydrogenation at 230 °C and 1.2 bar total pressure. This work paves the way for the optimization of the Mn/Co molar ratio and likely other chemical promoters toward low CH_4-selectvity and optimum chain growth probability for FTS at higher than 1.2 bar total pressure.

■ ASSOCIATED CONTENT

Supporting Information

The Supporting Information is available free of charge at https://pubs.acs.org/doi/10.1021/acscatal.4c07921.

Experimental details about hydrogen transient isothermal chemisorption, ^{12}CO/^{13}CO isotopic exchange, ^{13}CO-SSITKA and TIH/TPH following SSITKA. HRTEM images, EDX and SAED patterns of unpromoted and Mn-promoted Co/γ-Al_2O_3 catalysts, H_2-TPD traces and amounts of chemisorbed H-s as a function of Mn/Co molar ratio, logarithmic plots of θ_{CO} for the determination of rate constant of CO-s desorption vs Mn/Co ratio, DRIFTS CO chemisorption under 5%CO/He and 5%CO/5 or 10%H_2/He adsorption gas compositions, ^{13}CO-SSITKA transient response curves in terms of dimensionless concentration (Z) and SSITKA kinetic parameters as a function of Mn/Co ratio and TOS in CO hydrogenation at 230 °C, logarithmic plots of the (1-Z$^{13}CH_4$) function vs time for kinetic modeling discrimination (methanation reaction), ASF plots as a function of Mn/Co ratio, CO−DRIFTS spectra recorded under transient isothermal hydrogenation of CO-s, plots of ln[α] versus time in 50% H_2/Ar gas stream for determination of the rate constant of hydrogenation of two linear-type CO-s to CH_4 (PDF)

■ AUTHOR INFORMATION

Corresponding Author

Angelos M. Efstathiou − *Department of Chemistry, Heterogeneous Catalysis Laboratory, University of Cyprus, CY 2109 Nicosia, Cyprus;* orcid.org/0000-0001-8393-8800; Email: efstath@ucy.ac.cy

Authors

Michalis A. Vasiliades − *Department of Chemistry, Heterogeneous Catalysis Laboratory, University of Cyprus,* *CY 2109 Nicosia, Cyprus;* orcid.org/0000-0002-1568-1158

Denzil Moodley − *Sasol Research and Technology, Sasolburg 1947, South Africa*

Renier Crous − *Sasol Research and Technology, Sasolburg 1947, South Africa*

Jana Potgieter − *Sasol Research and Technology, Sasolburg 1947, South Africa*

Thys Botha − *Sasol Research and Technology, Sasolburg 1947, South Africa*

Complete contact information is available at: https://pubs.acs.org/10.1021/acscatal.4c07921

Notes

The authors declare no competing financial interest.

■ ACKNOWLEDGMENTS

The SASOL South Africa Ltd. (Contract No. 123/17 GT) and the Research Committee of the University of Cyprus are gratefully acknowledged for the financial support of this work.

■ REFERENCES

(1) Gholami, Z.; Tišler, Z.; Rubáš, V. Recent advances in Fischer−Tropsch synthesis using cobalt-based catalysts: a review on supports, promoters, and reactors. *Catal. Rev. Sci. Eng.* **2021**, *63*, 512−595.

(2) Yahyazadeh, A.; Dalai, A. K.; Ma, W.; Zhang, L. Fischer−Tropsch synthesis for light olefins from syngas: a review of catalyst development. *Reactions* **2021**, *2*, 227−257.

(3) Ail, S. S.; Dasappa, S. Biomass to liquid transportation fuel via Fischer−Tropsch synthesis − Technology review and current scenario. *Renew. Sustain. Energy Rev.* **2016**, *58*, 267−286.

(4) Jahangiri, H.; Bennett, J.; Mahjoubi, P.; Wilson, K.; Gu, S. A review of advanced catalyst development for Fischer−Tropsch synthesis of hydrocarbons from biomass derived syn-gas. *Catal. Sci. Technol.* **2014**, *4*, 2210−2229.

(5) Fischer, N.; Claeys, M. In situ characterization of Fischer−Tropsch catalysts: a review. *J. Phys. D Appl. Phys.* **2020**, *53*, No. 293001.

(6) Khodakov, A. Y.; Chu, W.; Fongarland, P. Advances in the development of novel cobalt Fischer−Tropsch catalysts for synthesis of long-chain hydrocarbons and clean fuels. *Chem. Rev.* **2007**, *107*, 1692−1744.

(7) Kimpel, T. F.; Liu, J.; Chen, W.; Pestman, R.; Hensen, E. J. M. Pressure dependence and mechanism of Mn promotion of silica-supported Co catalyst in the Fischer−Tropsch reaction. *J. Catal.* **2023**, *425*, 181−195.

(8) Koshy, D. M.; Johnson, G. R.; Bustillo, K. C.; Bell, A. T. Scanning Nanobeam Diffraction and Energy Dispersive Spectroscopy Characterization of a Model Mn-Promoted Co/Al_2O_3 Nanosphere Catalyst for Fischer−Tropsch Synthesis. *ACS Catal.* **2020**, *10*, 12071−12079.

(9) Krylova, A. Y. Products of the Fischer−Tropsch synthesis (A Review). *Solid Fuel Chem.* **2014**, *48*, 22−35.

(10) Todic, B.; Ma, W.; Jacobs, G.; Davis, B. H.; Bukur, D. B. CO-insertion mechanism based kinetic model of the Fischer−Tropsch synthesis reaction over Re-promoted Co catalyst. *Catal. Today* **2014**, *228*, 32−39.

(11) Eschemann, T. O.; Oenema, J.; de Jong, K. P. Effects of noble metal promotion for Co/TiO_2 Fischer−Tropsch catalysts. *Catal. Today* **2016**, *261*, 60−66.

(12) Wang, Y.; Yang, X.; Xiao, L.; Qi, Y.; Yang, J.; Zhu, Y.-A.; Holmen, A.; Xiao, W.; Chen, D. Descriptor-Based Microkinetic Modeling and Catalyst Screening for CO Hydrogenation. *ACS Catal.* **2021**, *11*, 14545−14560.

(13) Tucker, C. L.; Ragoo, Y.; Mathe, S.; Macheli, L.; Bordoloi, A.; Rocha, T. C. R.; Govender, S.; Kooyman, P. J.; van Steen, E. Manganese promotion of a cobalt Fischer−Tropsch catalyst to improve operation at high conversion. *J. Catal.* **2022**, *411*, 97−108.

(14) Morales, F.; De Smit, E.; De Groot, F. M. F.; Visser, T.; Weckhuysen, B. M. Effects of manganese oxide promoter on the CO and H_2 adsorption properties of titania-supported cobalt Fischer−Tropsch catalysts. *J. Catal.* **2007**, *246*, 91−99.

(15) Rahmati, M.; Huang, B.; Mortensen, M. K.; Keyvanloo, K.; Fletcher, T. H.; Woodfield, B. F.; Hecker, W. C.; Argyle, M. D. Effect of different alumina supports on performance of cobalt Fischer−Tropsch catalysts. *J. Catal.* **2018**, *359*, 92−100.

(16) Jiang, F.; Wang, S.; Zheng, J.; Liu, B.; Xu, Y.; Liu, X. Fischer−Tropsch synthesis to lower α-olefins over cobalt-based catalysts: Dependence of the promotional effect of promoter on supports. *Catal. Today* **2021**, *369*, 158−166.

(17) Gavrilović; Save; Blekkan. The effect of potassium on cobalt-based Fischer−Tropsch catalysts with different cobalt particle sizes. *Catalysts* **2019**, *9*, 351.

(18) Jongsomjit, B.; Panpranot, J.; Goodwin, J. G. Effect of zirconia-modified alumina on the properties of Co/γ-Al_2O_3 catalysts. *J. Catal.* **2003**, *215*, 66−77.

(19) van Dijk, H. A. J.; Hoebink, J. H. B. J.; Schouten, J. C. Steady-state isotopic transient kinetic analysis of the Fischer−Tropsch synthesis reaction over cobalt-based catalysts. *Chem. Eng. Sci.* **2001**, *56*, 1211−1219.

(20) Horáček, J. Fischer−Tropsch synthesis, the effect of promoters, catalyst support, and reaction conditions selection. *Monatsh. Chem.* **2020**, *151*, 649−675.

(21) Deutschmann, O.; Knözinger, H.; Kochloefl, K.; Turek, T. Heterogeneous catalysis and solid catalysts, 2. Development and types of solid catalysts, in: *Ullmann's Encycl. Ind. Chem.*; Wiley-VCH Verlag GmbH & Co. KGaA: Weinheim, Germany, 2011.

(22) Morales, F.; Weckhuysen, B. M. Promotion effects in Co-based Fischer−Tropsch catalysis. *Catalysis* **2006**, *19*, 1−40.

(23) Xu, R.; Hou, C.; Xia, G.; Sun, X.; Li, M.; Nie, H.; Li, D. Effects of Ag promotion for Co/Al_2O_3 catalyst in Fischer−Tropsch synthesis. *Catal. Today* **2020**, *342*, 111−114.

(24) Mirzaei, A. A.; Arsalanfar, M.; Bozorgzadeh, H. R.; Samimi, A. A review of Fischer−Tropsch synthesis on the cobalt based catalysts. *Phys. Chem. Res.* **2014**, *2*, 179−201.

(25) Badoga, S.; Kamath, G.; Dalai, A. Effects of promoters (Mn, Mg, Co and Ni) on the Fischer−Tropsch activity and selectivity of KCuFe/mesoporous-alumina catalyst. *Appl. Catal. A Gen.* **2020**, *607*, No. 117861.

(26) Shimura, K.; Miyazawa, T.; Hanaoka, T.; Hirata, S. Fischer−Tropsch synthesis over alumina supported cobalt catalyst: Effect of promoter addition. *Appl. Catal. A Gen.* **2015**, *494*, 1−11.

(27) Chen, H.; Lian, Z.; Zhao, X.; Wan, J.; Pieters, P. F.; Oliver-Meseguer, J.; Yang, J.; Pach, E.; Carenco, S.; Treps, L.; Liakakos, N.; Shan, Y.; Altoe, V.; Wong, E.; Zhuo, Z.; Yang, F.; Su, J.; Guo, J.; Blum, M.; Lapidus, S. H.; Hunt, A.; Waluyo, I.; Ogasawara, H.; Zheng, H.; Yang, P.; Bell, A. T.; López, N.; Salmeron, M. The role of manganese in CoMnOx catalysts for selective long-chain hydrocarbon production via Fischer−Tropsch synthesis. *Nat. Commun.* **2024**, *15*, 10294.

(28) Kimpel, T. F. Structure Sensitivity of Manganese-Promoted Cobalt Fischer−Tropsch Synthesis Catalysts. PhD Thesis, Eindhoven University of Technology, 2023.

(29) Bezemer, G. L.; Radstake, P. B.; Falke, U.; Oosterbeek, H.; Kuipers, H. P. C. E.; van Dillen, A. J.; de Jong, K. P. Investigation of promoter effects of manganese oxide on carbon nanofiber-supported cobalt catalysts for Fischer−Tropsch synthesis. *J. Catal.* **2006**, *237*, 152−161.

(30) Morales, F.; Grandjean, D.; Mens, A.; de Groot, F. M. F.; Weckhuysen, B. M. X-ray absorption spectroscopy of Mn/Co/TiO_2 Fischer−Tropsch catalysts: Relationships between preparation method, molecular structure, and catalyst performance. *J. Phys. Chem. B* **2006**, *110*, 8626−8639.

(31) Feltes, T. E.; Espinosa-Alonso, L.; Smit, E. d.; D'Souza, L.; Meyer, R. J.; Weckhuysen, B. M.; Regalbuto, J. R. Selective adsorption

of manganese onto cobalt for optimized Mn/Co/TiO_2 Fischer−Tropsch catalysts. *J. Catal.* **2010**, *270*, 95−102.

(32) Zhu, M.-L.; Liu, X.; Niu, Y.; Yang, G.-Q.; Bao, J.; Song, Y.-H.; Yan, Y.-F.; Du, N.; Shui, M.-L.; Zhu, K.; Zhang, B.; Liu, Z.-T.; Ma, D.; Liu, Z.-W. Long-chain α-olefins production over Co-MnO_x catalyst with optimized interface. *Appl. Catal. B Environmental and Energy* **2024**, *346*, No. 123783.

(33) Ciufo, R. A.; Han, S.; Floto, M. E.; Henkelman, G.; Mullins, C. B. Low temperature dissociation of CO on manganese promoted cobalt (poly). *Chem. Commun.* **2020**, *56*, 2865−2868.

(34) Zhao, M.; Li, Y.; Zhao, Z.; Lyu, Y.; Lu, W.; Zhu, H.; Ding, Y. Mn doping of Co-Al spinel as Fischer−Tropsch catalyst support. *Appl. Catal. A: Gen.* **2021**, *624*, No. 118308.

(35) Xu, M.; Qin, X.; Xu, Y.; Zhang, X.; Zheng, L.; Liu, J.-X.; Wang, M.; Liu, X.; Ma, D. Boosting CO hydrogenation towards C_{2+} hydrocarbons over interfacial TiO_{2-x}/Ni catalysts. *Nat. Commun.* **2022**, *13*, 6720.

(36) Dinse, A.; Aigner, M.; Ulbrich, M.; Johnson, G. R.; Bell, A. T. Effects of Mn promotion on the activity and selectivity of Co/SiO_2 for Fischer−Tropsch Synthesis. *J. Catal.* **2012**, *288*, 104−114.

(37) Johnson, G. R.; Werner, S.; Bell, A. T. An Investigation into the effects of Mn promotion on the activity and selectivity of Co/SiO_2 for Fischer−Tropsch synthesis: Evidence for enhanced CO adsorption and dissociation. *ACS Catal.* **2015**, *5*, 5888−5903.

(38) den Breejen, J. P.; Frey, A. M.; Yang, J.; Holmen, A.; van Schooneveld, M. M.; de Groot, F. M. F.; Stephan, O.; Bitter, J. H.; de Jong, K. P. A highly active and selective manganese oxide promoted Cobalt-on-silica Fischer−Tropsch catalyst. *Top. Catal.* **2011**, *54*, 768−777.

(39) Johnson, G. R.; Bell, A. T. Effects of Lewis acidity of metal oxide promoters on the activity and selectivity of Co-based Fischer−Tropsch synthesis catalysts. *J. Catal.* **2016**, *338*, 250−264.

(40) Potgieter, J. H.; Moodley, D.; Botha, T.; Visagie, J.; Manong, T.; Frank, M.; Claeys, M.; van Steen, E.; Böltken, T.; Pfeifer, P. Development of promoted cobalt/alumina Fischer−Tropsch catalysts for increased activity and selectivity: Micro-reactor to piloting scale. *Catal. Today* **2024**, *432*, No. 114554.

(41) Moodley, D.; Botha, T.; Crous, R.; Potgieter, J.; Visagie, J.; Walmsley, R.; Dwyer, C. Catalysis for Sustainable Aviation Fuels: Focus on Fischer−Tropsch Catalysis. In *Catalysis for a Sustainable Environment: Reactions, Processes, and Applied Technologies*; Pombeiro, A. J. L.; Sutradhar, M.; Alegria, E. C. B. A, Eds.; Wiley, 2024; pp 73−116.

(42) Chen, W.; Kimpel, T. F.; Song, Y.; Chiang, F.; Zijlstra, B.; Pestman, R.; Wang, P.; Hensen, E. J. M. Influence of carbon deposits on the Cobalt-catalyzed Fischer−Tropsch reaction: Evidence of a two-site reaction model. *ACS Catal.* **2018**, *8*, 1580−1590.

(43) Pansare, S.; Sirijaruphan, A.; Goodwin, J. G. Investigation of Reaction at the Site Level Using SSITKA. *in: Isot. Heterog. Catal.* **2006**, *4*, 183−211.

(44) Petallidou, K. C.; Vasiliades, M. A.; Efstathiou, A. M. Deactivation of Co/γ-Al_2O_3 in CO methanation studied by transient isotopic experiments: The effect of Co particle size. *J. Catal.* **2020**, *389*, 176−194.

(45) Vasiliades, M. A.; Kyprianou, K. K.; Govender, N. S.; Govender, A.; Crous, R.; Moodley, D.; Efstathiou, A. M. The effect of CO partial pressure on important kinetic parameters of methanation reaction on Co-Based FTS catalyst studied by SSITKA-MS and operando DRIFTS-MS techniques. *Catalysts* **2020**, *10* (5), 583.

(46) Chen, W.; Filot, I. A. W.; Pestman, R.; Hensen, E. J. M. Mechanism of Cobalt-catalyzed CO hydrogenation: 2. Fischer−Tropsch synthesis. *ACS Catal.* **2017**, *7*, 8061−8071.

(47) Lorito, D.; Paredes-Nunez, A.; Mirodatos, C.; Schuurman, Y.; Meunier, F. C. Determination of formate decomposition rates and relation to product formation during CO hydrogenation over supported cobalt. *Catal. Today* **2016**, *259*, 192−196.

(48) Paredes-Nunez, A.; Lorito, D.; Guilhaume, N.; Mirodatos, C.; Schuurman, Y.; Meunier, F. C. Nature and reactivity of the surface species observed over a supported cobalt catalyst under CO/H_2 mixtures. *Catal. Today* **2015**, *242*, 178−183.

(49) Vasiliades, M. A.; Govender, N. S.; Govender, A.; Crous, R.; Moodley, D.; Botha, T.; Efstathiou, A. M. The effect of H_2 pressure on the carbon path of methanation reaction on Co/γ-Al_2O_3: Transient isotopic and operando methodology studies. *ACS Catal.* **2022**, *12*, 15110−15129.

(50) Frøseth, V.; Storsæter, S.; Borg, Ø; Blekkan, E. A.; Rønning, M.; Holmen, A. Steady state isotopic transient kinetic analysis (SSITKA) of CO hydrogenation on different Co catalysts. *Appl. Catal. A. Gen.* **2005**, *289*, 10−15.

(51) Enger, B. C.; Frøseth, V.; Yang, J.; Rytter, E.; Holmen, A. SSITKA analysis of CO hydrogenation on Zn modified cobalt catalysts. *J. Catal.* **2013**, *297*, 187−192.

(52) Carvalho, A.; Ordomsky, V. V.; Luo, Y.; Marinova, M.; Muniz, A. R.; Marcilio, N. R.; Khodakov, A. Y. Elucidation of deactivation phenomena in cobalt catalyst for Fischer−Tropsch synthesis using SSITKA. *J. Catal.* **2016**, *344*, 669−679.

(53) Vasiliades, M. A.; Kalamaras, C. M.; Govender, N. S.; Govender, A.; Efstathiou, A. M. The effect of preparation route of commercial Co/γ-Al_2O_3 catalyst on important Fischer−Tropsch kinetic parameters studied by SSITKA and CO-DRIFTS transient hydrogenation techniques. *J. Catal.* **2019**, *379*, 60−77.

(54) Ledesma, C.; Yang, J.; Chen, D.; Holmen, A. Recent approaches in mechanistic and kinetic studies of catalytic reactions using SSITKA technique. *ACS Catal.* **2014**, *4*, 4527−4547.

(55) Biloen, P.; Helle, J. N.; van den Berg, F. G. A.; Sachtler, W. M. H. On the activity of Fischer−Tropsch and methanation catalysts: A study utilizing isotopic transients. *J. Catal.* **1983**, *81*, 450−463.

(56) Shannon, S. L.; Goodwin, J. G. Characterization of catalytic surfaces by isotopic-transient kinetics during steady-state reaction. *Chem. Rev.* **1995**, *95*, 677−695.

(57) Janssens, P.; Poissonnier, J.; Chakkingal, A.; Bos, R.; Thybaut, J. W. Recent advances in the use of steady-state isotopic transient kinetic analysis data in (micro)kinetic modeling for catalyst and process design. *Catal. Commun.* **2023**, *179*, No. 106688.

(58) Balakos, M. W.; Chuang, S. S. C.; Srinivas, G.; Brundage, M. A. Infrared study of the dynamics of adsorbed species during CO hydrogenation. *J. Catal.* **1995**, *157*, 51−65.

(59) Efstathiou, A. M. Elucidation of mechanistic and kinetic aspects of water-gas shift reaction on supported Pt and Au catalysts via transient isotopic techniques. *Catalysis* **2016**, *28*, 175−236.

(60) Schweicher, J.; Bundhoo, A.; Frennet, A.; Kruse, N.; Daly, H.; Meunier, F. C. DRIFTS/MS Studies during chemical transients and SSITKA of the CO/H_2 reaction over Co-MgO catalysts. *J. Phys. Chem. C* **2010**, *114*, 2248−2255.

(61) El-Roz, M.; Bazin, P.; Daturi, M.; Thibault-Starzyk, F. Operando Infrared (IR) Coupled to Steady-State Isotopic Transient Kinetic Analysis (SSITKA) for Photocatalysis: Reactivity and Mechanistic Studies. *ACS Catal.* **2013**, *3*, 2790−2798.

(62) Holmen, A.; Yang, J.; Chen, D. Steady-State Isotopic Transient Kinetic Analysis (SSITKA). In *Handbook of Advanced Catalyst Characterization*; Wachs, I. E.; Bañares, M. A., Eds.; Spinger Nature: Switzerland AG, 2023.

(63) Van Santen, R. A.; Markvoort, A. J.; Filot, I. A. W.; Ghouri, M. M.; Hensen, E. J. M. Mechanism and microkinetics of the Fischer−Tropsch reaction. *Phys. Chem. Chem. Phys.* **2013**, *15*, 17038−17063.

(64) Moazami, N.; Wyszynski, M. L.; Rahbar, K.; Tsolakis, A.; Mahmoudi, H. A comprehensive study of kinetics mechanism of Fischer−Tropsch synthesis over cobalt-based catalyst. *Chem. Eng. Sci.* **2017**, *171*, 32−60.

(65) Teimouri, Z.; Abatzoglou, N.; Dalai, A. K. Kinetics and selectivity study of Fischer−Tropsch synthesis to C5+ hydrocarbons: A review. *Catalysts* **2021**, *11* (3), 330.

(66) Pedersen, E.-Ø.; Svenum, I.-H.; Blekkan, E. A. Mn promoted Co catalysts for Fischer−Tropsch production of light olefins − An experimental and theoretical study. *J. Catal.* **2018**, *361*, 23−32.

(67) Costa, C. N.; Christou, S. Y.; Georgiou, G.; Efstathiou, A. M. Mathematical modeling of the oxygen storage capacity phenomenon

studied by CO pulse transient experiments over Pd/CeO_2 catalyst. *J. Catal.* **2003**, *219*, 259−272.

(68) Zowtiak, J. M.; Bartholomew, C. H. The kinetics of H_2 adsorption on and desorption from cobalt and the effects of support thereon. *J. Catal.* **1983**, *83*, 107−120.

(69) Perego, C.; Peratello, S. Experimental methods in catalytic kinetics. *Catal. Today* **1999**, *52*, 133−145.

(70) Pestman, R.; Chen, W.; Hensen, E. Insight into the rate-determining step and active sites in the Fischer−Tropsch reaction over Cobalt catalysts. *ACS Catal.* **2019**, *9*, 4189−4195.

(71) Ojeda, M.; Nabar, R.; Nilekar, A. U.; Ishikawa, A.; Mavrikakis, M.; Iglesia, E. CO activation pathways and the mechanism of Fischer−Tropsch synthesis. *J. Catal.* **2010**, *272*, 287−297.

(72) Martinez, A.; Lopez, C.; Marquez, F.; Diaz, I. Fischer−Tropsch synthesis of hydrocarbons over mesoporous Co/SBA-15 catalysts: the influence of metal loading, cobalt precursor, and promoters. *J. Catal.* **2003**, *220*, 486−499.

(73) Li, H.; Wang, J.; Chen, C.; Jia, L.; Hou, B.; Li, D. Effects of macropores on reducing internal diffusion limitations in Fischer−Tropsch synthesis using a hierarchical cobalt catalyst. *RSC Adv.* **2017**, *7*, 9436−9445.

(74) Sasaki, S.; Suzuki, H.; Kimura, Y.; Sato, T.; Tanigaki, T.; Kido, O.; Kamitsuji, K.; Kurumada, M.; Kaito, C. Direct observation of the formation of alumina phase by metallic Al solid-SiO_2 solid reaction. *Earth, Planets Sp* **2005**, *57*, 399−401.

(75) Ma, J.; Guo, E.; Yin, L. Porous hierarchical spinel Mn-doped $NiCo_2O_4$ nanosheet architectures as high-performance anodes for lithium-ion batteries and electrochemical reaction mechanism. *J. Mater. Sci. Mater. Electron.* **2019**, *30*, 8555−8567.

(76) Johnson, G. R.; Werner, S.; Bustillo, K. C.; Ercius, P.; Kisielowski, C.; Bell, A. T. Investigations of element spatial correlation in Mn-promoted Co-based Fischer−Tropsch synthesis catalysts. *J. Catal.* **2015**, *328*, 111−122.

(77) Werner, S.; Johnson, G. R.; Bell, A. T. Synthesis and characterization of supported Cobalt-Manganese nanoparticles as model catalysts for Fischer−Tropsch synthesis. *ChemCatChem.* **2014**, *6*, 2881−2888.

(78) Johnson, G. R.; Werner, S.; Bell, A. T. An investigation into the effects of Mn promotion on the activity and selectivity of Co/SiO_2 for Fischer−Tropsch synthesis: Evidence for enhanced CO adsorption and dissociation. *ACS Catal.* **2015**, *5*, 5888−5903.

(79) Kantcheva, M.; Kucukkal, M. U.; Suzer, S. Spectroscopic investigation of species arising from CO chemisorption on Titania-supported manganese. *J. Catal.* **2000**, *190*, 144−156.

(80) Feltes, T. E.; Zhao, Y.; Klie, R. F.; Meyer, R. J.; Regalbuto, J. R. The influence of preparation method on Mn-Co interactions in Mn/Co/TiO_2 Fischer−Tropsch catalysts. *ChemCatChem.* **2010**, *2*, 1065−1068.

(81) Morales, F.; De groot, F. M. F.; Gijzeman, O. L. J.; Mens, A.; Stephan, O.; Weckhuysen, B. M. Mn promotion effects in Co/TiO_2 Fischer−Tropsch catalysts as investigated by XPS and STEM-EELS. *J. Catal.* **2005**, *230*, 301−308.

(82) Al-Senani, G. M.; Deraz, N. M.; Abd-Elkader, O. H. Magnetic and Characterization Studies of CoO/Co_3O_4 Nanocomposite. *Processes* **2020**, *8* (7), 844.

(83) Chen, X.; Yan, S.; Wang, N.; Peng, S.; Wang, C.; Hong, Q.; Zhang, X.; Dai, S. Facile synthesis and characterization of ultrathin δ-MnO_2 nanoflakes. *RSC Adv.* **2017**, *7*, 55734−55740.

(84) Shadravan, V.; Bukas, V. J.; Gunasooriya, G. T. K. K.; Waleson, J.; Drewery, M.; Karibika, J.; Jones, J.; Kennedy, E.; Adesina, A.; Norskov, J.; Stockenhuber, M. Effect of manganese on the selective catalytic hydrogenation of CO_x in the presence of light hydrocarbons over Ni/Al_2O_3: An experimental and computational study. *ACS Catal.* **2020**, *10*, 1535−1547.

(85) Morales, F.; de Groot, F. M. F.; Glatzel, P.; Kleimenov, E.; Bluhm, H.; Hävecker, M.; Knop-Gericke, A.; Weckhuysen, B. M. In situ X-ray absorption of Co/Mn/TiO_2 catalysts for Fischer−Tropsch synthesis. *J. Phys. Chem. B* **2004**, *108*, 16201−16207.

(86) van Koppen, L. M.; Iulian Dugulan, A.; Leendert Bezemer, G.; Hensen, E. J. M. Manganese as a structural promoter in silica-supported cobalt Fischer−Tropsch catalysts under simulated high conversion conditions. *J. Catal.* **2023**, *428*, No. 115173.

(87) Couble, J.; Bianchi, D. Heats of adsorption of linearly adsorbed CO species on Co^{2+} and C^{oo} sites of reduced Co/Al_2O_3 catalysts in relationship with the CO/H_2 reaction. *Appl. Catal. A. Gen.* **2012**, *445−446*, 1−13.

(88) Efstathiou, A. M.; Chafik, T.; Bianchi, D.; Bennett, C. O. A transient kinetic study of the CO/H_2 reaction on Rh/Al_2O_3 using FTIR and mass spectroscopy. *J. Catal.* **1994**, *148*, 224−239.

(89) Gopal, P. G.; Schneider, R. L.; Watters, K. L. Evidence for Production of Surface Formate upon Direct Reaction of CO with Alumina and Magnesia. *J. Catal.* **1987**, *105*, 366−372.

(90) Visconti, C. G.; Lietti, L.; Tronconi, E.; Forzatti, P.; Zennaro, R.; Finocchio, E. Fischer−Tropsch synthesis on a Co/Al_2O_3 catalyst with CO_2 containing syngas. *Appl. Catal. A: Gen.* **2009**, *355*, 61−68.

(91) Vada, S.; Chen, B.; Goodwin, J.G. Isotopic transient study of La Promotion of Co/Al_2O_3 for Co hydrogenation. *J. Catal.* **1995**, *153*, 224−231.

(92) den Breejen, J. P.; Radstake, P. B.; Bezemer, G. L.; Bitter, J. H.; Frøseth, V.; Holmen, A.; de Jong, K. P. On the origin of the cobalt particle size effects in Fischer−Tropsch catalysis. *J. Am. Chem. Soc.* **2009**, *131*, 7197−7203.

(93) den Breejen, J. P.; Sietsma, J. R. A.; Friedrich, H.; Bitter, J. H.; de Jong, K. P. Design of supported cobalt catalysts with maximum activity for the Fischer−Tropsch synthesis. *J. Catal.* **2010**, *270*, 146−152.

(94) Yang, X.; Yang, J.; Zhao, T.; Qian, W.; Wang, Y.; Holmen, A.; Jiang, W.; Chen, D.; Ben, H. Kinetic insights into the effect of promoters on Co/Al_2O_3 for Fischer−Tropsch synthesis. *Chem. Eng. J.* **2022**, *445*, No. 136655.

(95) Bal'zhinimaev, B. S.; Sadovskaya, E. M.; Suknev, A. P. Transient isotopic kinetics study to investigate reaction mechanisms. *Chem. Eng. J.* **2009**, *154*, 2−8.

(96) Bianchi, D.; Gass, J. L. Hydrogenation of carbonaceous adsorbed species on an iron/alumina catalyst I. Experiments in isothermal conditions and exploitation by a kinetic model. *J. Catal.* **1990**, *123*, 298−309.

(97) Efstathiou, A. M.; Chafik, T.; Bianchi, D.; Bennett, C. O. CO chemisorption and hydrogenation of surface carbon species formed after CO/He reaction on Rh/MgO: A transient kinetic study using FTIR and mass spectroscopy. *J. Catal.* **1994**, *147*, 24−37.

(98) Efstathiou, A. M.; Bennett, C. O. The CO/H_2 reaction on Rh/Al_2O_3. II: Kinetic study by transient isotopic methods. *J. Catal.* **1989**, *120*, 137−156.

(99) Frøseth, V.; Holmen, A. CO hydrogenation on Co/γ-Al_2O_3 and CoRe/γ-Al_2O_3 studied by SSITKA. *Top. Catal.* **2007**, *45*, 45−50.

(100) Schanke, D.; Vada, S.; Blekkan, E. A.; Hilmen, A. M.; Hoff, A.; Holmen, A. Study of Pt-promoted cobalt CO hydrogenation catalysts. *J. Catal.* **1995**, *156*, 85−95.

(101) Belambe, A. R.; Oukaci, R.; Goodwin, J. G. Effect of pretreatment on the activity of a Ru-promoted Co/Al_2O_3 Fischer−Tropsch catalyst. *J. Catal.* **1997**, *166*, 8−15.

(102) Tucker, C. L.; van Steen, E. Activity and selectivity of a cobalt-based Fischer−Tropsch catalyst operating at high conversion for once-through biomass-to-liquid operation. *Catal. Today* **2020**, *342*, 115−123.

(103) Ma, W.; Jacobs, G.; Ji, Y.; Bhatelia, T.; Bukur, D. B.; Khalid, S.; Davis, B. H. Fischer−Tropsch synthesis: Influence of CO conversion on selectivities, H_2/CO usage ratios, and catalyst stability for a Ru promoted Co/Al_2O_3 catalyst using a slurry phase reactor. *Top. Catal.* **2011**, *54*, 757−767.

(104) Bukur, D. B.; Pan, Z.; Ma, W.; Jacobs, G.; Davis, B. H. Effect of CO conversion on the product distribution of a Co/Al_2O_3 Fischer−Tropsch synthesis catalyst using a fixed bed reactor. *Catal. Lett.* **2012**, *142*, 1382−1387.

(105) Liu, Y.; He, C.; Jiang, X.; Zhang, R.; Liu, X.; Hildebrandt, D.; Lu, X. Fischer–Tropsch synthesis to α-Olefins with low CO_2 selectivity on a Co_2C catalyst. *Chem. Eng. J.* **2024**, *479*, No. 147927.

(106) Paredes-Nunez, A.; Lorito, D.; Schuurman, Y.; Guilhaume, N.; Meunier, F. C. Origins of the poisoning effect of chlorine on the CO hydrogenation activity of alumina-supported cobalt monitored by operando FT-IR spectroscopy. *J. Catal.* **2015**, *329*, 229–236.

(107) Daly, H.; Ni, J.; Thompsett, D.; Meunier, F. C. On the usefulness of carbon isotopic exchange for the operando analysis of metal–carbonyl bands by IR over ceria-containing catalysts. *J. Catal.* **2008**, *254*, 238–243.

(108) Weststrate, C. J.; van de Loosdrecht, J.; Niemantsverdriet, J. W. Spectroscopic insights into cobalt-catalyzed Fischer–Tropsch synthesis: A review of the carbon monoxide interaction with single crystalline surfaces of cobalt. *J. Catal.* **2016**, *342*, 1–16.

(109) Kollár, M.; De Stefanis, A.; Solt, H. E.; Mihályi, M. R.; Valyon, J.; Tomlinson, A. A. G. The mechanism of the Fischer–Tropsch reaction over supported cobalt catalysts. *J. Mol. Catal. A Chem.* **2010**, *333*, 37–45.

(110) McNab, A. I.; McCue, A. J.; Dionisi, D.; Anderson, J. A. Quantification and qualification by in-situ FTIR of species formed on supported-cobalt catalysts during the Fischer–Tropsch reaction. *J. Catal.* **2017**, *353*, 286–294.

(111) Nonneman, L. E. Y.; Ponec, V. Promotion and support effects in syngas reactions. *Catal. Lett.* **1991**, *7*, 197–203.